# Nanomaterial-based contrast agents

**Jessica C. Hsu**[1,2], **Zhongmin Tang**[2], **Olga E. Eremina**[3], **Alexandros Marios Sofias**[4], **Twan Lammers**[4], **Jonathan F. Lovell**[5], **Cristina Zavaleta**[3], **Weibo Cai**[2], **David P. Cormode**[1,✉]

[1]Department of Radiology, University of Pennsylvania, Philadelphia, PA, USA.

[2]Departments of Radiology and Medical Physics, University of Wisconsin-Madison, Madison, WI, USA.

[3]Department of Biomedical Engineering, University of Southern California, Los Angeles, CA, USA.

[4]Department of Nanomedicine and Theranostics, Institute for Experimental Molecular Imaging, Faculty of Medicine, RWTH Aachen University, Aachen, Germany.

[5]Department of Biomedical Engineering, University at Buffalo, State University of New York, Buffalo, NY, USA.

## Abstract

Medical imaging, which empowers the detection of physiological and pathological processes within living subjects, has a vital role in both preclinical and clinical diagnostics. Contrast agents are often needed to accompany anatomical data with functional information or to provide phenotyping of the disease in question. Many newly emerging contrast agents are based on nanomaterials as their high payloads, unique physicochemical properties, improved sensitivity and multimodality capacity are highly desired for many advanced forms of bioimaging techniques and applications. Here, we review the developments in the field of nanomaterial-based contrast agents. We outline important nanomaterial design considerations and discuss the effect on their physicochemical attributes, contrast properties and biological behaviour. We also describe commonly used approaches for formulating, functionalizing and characterizing these nanomaterials. Key applications are highlighted by categorizing nanomaterials on the basis of their X-ray, magnetic, nuclear, optical and/or photoacoustic contrast properties. Finally, we offer our perspectives on current challenges and emerging research topics as well as expectations for future advancements in the field.

✉ david.cormode@pennmedicine.upenn.edu .

## Introduction

Contrast agents can be used in imaging procedures to enhance the detectability of underlying tissue anatomy or to derive information about certain pathological processes. These agents have traditionally been based on small molecules such as gadolinium chelates or iodinated small molecules, but their use has been restricted to a relatively small number of imaging applications, such as blood pool or urinary tract imaging. Therefore, much of the research in recent decades has been devoted to improving current designs and developing alternative contrast agents, such as nanomaterial-based formulations with novel compositions and structures. Nano-based contrast agents have performed well in a number of advanced biomedical applications, such as cell tracking, intraoperative tumour detection and implant monitoring[1,2].

There are several criteria to consider when designing nanomaterial-based contrast agents for specific bioimaging applications[3] (Fig. 1). First, nano-based contrast agents are typically in the 1–400 nm size range, but their size can be tuned to exhibit very different behaviours in vivo. Sub-5-nm nanoparticles (NPs) tend to rapidly clear via kidney filtration to prevent long-term retention in the mononuclear phagocyte system (MPS) organs[4–6], whereas larger NPs may remain in the body longer. NPs can accumulate in some diseased tissues via processes such as the enhanced permeation and retention (EPR) effect if long-circulating, receptor-specific uptake if targeted or opsonization by plasma proteins and others[7–10]. Size may also affect the contrast properties of an NP platform; for instance, the fluorescence emission wavelength of quantum dots (QDs) generally increases with increasing core diameter[11]. Nano-based contrast agents are mostly spherical in shape, but can also be formed as rods, stars or other shapes, which can determine their imaging utility and avidity in target binding. For example, gold nanostars have a high surface-to-core ratio for improved ligand conjugation, and the tips of their points exhibit enhanced Raman spectra for effective surface-enhanced Raman spectroscopy (SERS)-based imaging[12]. Next, materials that can generate or enhance contrast, such as metals, fluorescent probes and radionuclides, can be incorporated into the core, integrated in the shell or attached to the surface or coating of the NP. Notably, NPs carry more contrast payloads per entity compared with conventional small molecules, resulting in image contrast of higher intensity[13]. Contrast agents can be encapsulated in or bound to larger carrier structures, such as liposomes, dendrimers, polymers and silica, to facilitate desired circulation half-lives for specific applications, biodegradability and colloidal stability[14]. NP surfaces can be easily modified with coating ligands, such as neutrally charged polyethylene glycol (PEG), that yield varying pharmacokinetic and biodistribution profiles[15]. The surface can also be functionalized with drugs or nucleic acids for therapeutic effects, or targeting moieties, such as antibodies and peptides, for targeted imaging.

Nano-based contrast agents can be used for many major medical imaging modalities[16–18], as summarized in Table 1 and Fig. 1. Computed tomography (CT) generates image contrast on the basis of differential mass-dependent absorption or scattering of ionizing X-ray radiation. Although non-contrast enhanced CT is effective for imaging electron-dense tissues, such as bones and calcifications, and non-dense tissues, such as lungs, distinguishing soft tissues without the use of exogenous contrast agents is difficult. The earliest reports of nano-based

CT contrast agents were based on emulsions or liposomes containing clinically approved iodinated molecules[19–21]. Subsequent formulations typically involve high atomic number (Z) elements such as cerium, gold and bismuth[22,23]. Contrast-enhanced mammography, or dual-energy mammography (DEM), is a clinical tool that improves lesion detection in dense breasts. Breast imaging via DEM uses lower X-ray energy spectra compared with CT; therefore, lower Z elements, such as silver and molybdenum, would be suited for development into DEM-specific nano-based contrast agents[24,25].

Magnetic resonance imaging (MRI) is a non-ionizing modality that generates tissue contrast on the basis of the relaxation processes of neighbouring water protons in the presence of an external magnetic field. Most MR contrast agents are either paramagnetic, which yields contrast for $T_1$ (longitudinal)-weighted imaging, or superparamagnetic, which provides contrast in $T_2/T_2{}^*$ (transverse)-weighted imaging (where $T_1$ and $T_2$ are the water relaxation times). Notably, by modulating the core size, the same type of nano-based contrast agent can be used for either $T_1$-weighted or $T_2$-weighted imaging[26]. $T_1$ agents, such as those based on gadolinium and manganese, result in positive contrast (brightening) on MR images[27], whereas $T_2$-shortening agents, such as iron oxide nanoparticles (IONPs), give rise to negative contrast (darkening) on MR images[28,29]. IONPs have shown promise in clinical diagnosis as they are frequently used as an 'off-label' MR contrast agent. Another class of MR agent, which does not rely on proton relaxivity, produces a signal through chemical exchange saturation transfer (CEST) by enhancing the difference in the chemical shift of exchangeable protons. CEST agents can be classified as paramagnetic (PARACEST) agents that involve paramagnetic lanthanide ions, such as europium and ytterbium, or diamagnetic (diaCEST) agents that involve liposomes or polymers[30,31]. One advantage of CEST is the ability to turn the contrast on or off depending on the pulse sequence used, which allows for hot-spot imaging. However, it is of lower sensitivity than conventional MRI. Another variant of MRI is $^{19}F$ MRI, in which specialized coils are used to detect signal from agents loaded with fluorine. As humans have low levels of fluorine, this also results in hot-spot imaging. $^{19}F$ MRI agents are usually emulsions or NPs composed of inorganic fluoride salts[32,33]. Drawbacks of $^{19}F$ MRI include lower sensitivity compared with conventional MRI and the need for additional equipment. Magnetic particle imaging (MPI) is a recently developed technique in which a shaped magnetic field is scanned over the region of interest[34]. Magnetic NPs can be detected by this technique, owing to signals emitted when they enter the field-free zone as the field moves. MPI is a high spatial resolution, temporal resolution and sensitivity technique[35] that provides readouts on the spatial distribution of magnetic NPs, such as IONPs, but as it offers no signal from endogenous tissue, it is often paired with another technique, such as CT, to provide anatomical information. Limitations of MPI include sparse preclinical availability and a lack of widespread clinical use.

Nuclear imaging approaches, including positron emission tomography (PET) and single photon emission computed tomography (SPECT), are based on the detection of ionizing γ-photons emitted from radionuclides during radioactive decay. PET signals arise from electron–positron annihilation that releases two γ-rays travelling in opposite directions[36]. PET imaging is an appealing approach for measuring NP biodistribution in vivo over time[37]. SPECT has the potential for multiplexed imaging owing to its ability to discriminate isotopes based on the characteristic energies of emitted γ-photons. Essentially, any

nanomaterial can be modified with radioisotopes through chelation, intrinsic labelling and chelator-free post-synthetic labelling[38]. Commonly used radioisotopes for NP imaging include $^{64}$Cu and $^{89}$Zr for PET imaging and $^{99m}$Tc and $^{111}$In for SPECT imaging[39]. Although nuclear imaging suffers from much lower spatial resolution, it has a better detection limit towards its contrast agents than MRI and CT.

Fluorescence imaging is a rapid, high-throughput modality that detects photon emission in the visible or near-infrared (NIR) range upon energetic excitation. This technique offers real-time imaging and is highly sensitive towards contrast agents but has low depth penetration (<1 cm) owing to visible light absorption and scattering in tissues. To improve tissue penetration issues, NIR emitting semiconducting QDs, such as those based on cadmium selenide (CdSe) and silver sulfide ($Ag_2S$), can be synthesized as tissue absorbs less light in the NIR region[40]. The NIR range is further categorized into NIR-I (700–950 nm) and NIR-II (1,000–1,700 nm) windows, where the latter is more advantageous for bioimaging owing to lower tissue autofluorescence and photon scattering and absorption, thus achieving higher signal-to-noise ratio (SNR) and deeper tissue penetration. Owing to the quantum confinement effect, the core size of a QD dictates their absorbance and emission wavelengths[41]. Other frequently reported nano-based fluorescent or optical agents include gold nanoparticles (AuNPs), fluorophore-conjugated polymer-based or lipid-based NPs, carbon nanomaterials and lanthanide-doped upconverting NPs.

Photoacoustic imaging (PAI), also known as optoacoustic imaging, is based on the generation of broadband ultrasonic waves from transient thermoelastic expansion of tissues upon direct laser light irradiation. PAI is less limited by tissue thickness and thus achieves better penetration depth (<5 cm) compared with conventional optical imaging techniques. Exogenous nano-based PA contrast agents have been engineered to possess efficient photothermal conversion, high photostability and optimal NIR absorption with large cross-sections[42]. These agents include gold nanostructures, $Ag_2S$ NPs, dye-decorated nanomaterials and semiconducting polymeric NPs[43,44].

Ultrasound imaging uses hand-held transducers that emit sound waves that are typically in the 1–20 MHz range. These sound waves are reflected, scattered or absorbed by tissues and tissue interfaces. From the sound waves that return to the transducer, images of the subject can be formed. Ultrasound provides high spatial and temporal resolution, is portable and low cost and is widely available. On the contrary, it is operator-dependent, has low soft tissue contrast and provides limited fields of view. Contrast agents for ultrasound have historically been based on gas microbubbles[45], which are outside the scope of this Primer. However, in recent years, contrast agents for ultrasound based on nanobubbles have been reported. These structures are composed of a gas core, which is often a perfluorocarbon, enclosed in a shell made of lipids, polymers or proteins[46].

This Primer aims to inspect the different facets of bioimaging using nanomaterial-based contrast agents and should give readers the tools to design and evaluate nanomaterials as contrast agents. The Primer examines various synthetic approaches used to produce nano-based contrast agent platforms by focusing on their primary design considerations. The array of analytical techniques used for characterizing NP formulations and assessing their

contrast properties among other attributes is outlined, and the main biomedical applications of nano-based contrast agents, including structural and functional imaging, are highlighted using relevant examples. Key factors that affect the reproducibility of nanomaterials and reliability of data are described, and potential guidelines and repositories for data reporting are discussed. Finally, the Primer offers perspectives on current challenges and future developments in the field of nano-based contrast agents.

## Experimentation

Some of the most frequently studied nano-based contrast agent formulations for medical imaging applications include inorganic solid core NPs (for example, metal and metal alloy), lipid-based structures (for example, liposomes, emulsions, micelles and lipoproteins), polymeric NPs (for example, PEG, dextran and synthetic polymers) or a combination of these different NPs. This section details the various synthetic strategies and purification approaches, as well as surface modification and conjugation methods, that are most commonly implemented to fabricate these nano-based contrast agents (Fig. 2). Recent advances in synthetic techniques are also discussed, and factors dictating the design of an NP contrast agent are described.

### Nanoparticle synthesis

At the broadest level, NP synthesis can be classified as top-down (milling) or bottom-up (self-assembly), of which the latter is more commonly used for contrast agents. The top-down approach involves ball milling, laser ablation, photolithography or sputter deposition to derive NPs from bulk materials. These physical processes are not cost-effective as they require expensive and complicated instruments, as well as high power consumption. On the contrary, bottom-up syntheses entail the ionization of precursor chemicals in liquid or vapour phase, which leads to the nucleation and growth of nuclei into nanoclusters, or other approaches such as precipitation or self-assembly. For low-cost, high-throughput fabrication of nano-based contrast agents, aqueous syntheses are ideal as they use fewer toxic reactants and are simple, economical, energy-efficient and eco-friendly. In many cases, hydrophobic or organic syntheses are adopted to control the nanomaterial size, composition and shape with high precision. However, subsequent surface modification is necessary to improve the solubility and stability of the obtained nanostructures. Recently, there has been growing interest in applying natural templates, green chemistry, microfluidics and artificial intelligence for NP synthesis[47–50] (Fig. 2a). Nevertheless, NP formulation methodology and the required associated apparatus are highly specific to each NP type.

**Inorganic nanocrystals.**—Inorganic nanocrystals are typically synthesized from a mixture of metal salts and capping ligands either in the aqueous or hydrophobic phase[51]. For instance, the most commonly used method to synthesize AuNPs is that of Turkevich, which involves adding a reducing agent (for example, sodium citrate) to an aqueous gold salt. The size of AuNPs can be fine-tuned by varying the amount of reductants used or by using reductants with different reducing strengths — stronger reducing agents typically result in smaller NPs (for example, sodium borohydride versus hydroquinone)[52]. Furthermore, the Brust method transfers gold salts from water to toluene or other organic solvents, while

capping AuNPs (1–5 nm) with dodecanethiol or other hydrophobic ligands[53]. With this method, the core size can be controlled by adjusting the amount of ligands used in the synthesis. The morphology can also be tuned by adding cetyl trimethylammonium bromide to gold seeds to produce gold nanorods (AuNRs) or nanostars[54] or by depositing gold seeds onto a template (for example, silica spheres) to yield gold nanocages or nanoshells[55].

Many hydrophobic phase-based syntheses have been established to produce various metal nanocrystals with controllable and monodisperse diameters. For example, iron salts are reacted with sodium oleate to form iron oleate complexes, which are then slowly heated in octadecene to produce oleic-acid-coated iron oxide cores[56]. The same strategy has been adapted to form manganese oxide (MnO) NPs by using manganese precursor salts[57]. Furthermore, methods such as hot injection and thermal decomposition can be used to synthesize conventional QDs with tunable fluorescence emission spectra and high quantum yields following a similar procedure. For example, a solution of cadmium and selenium precursor salts is quickly injected into hot trioctylphosphine oxide solvent to fabricate CdSe QDs with low size dispersity[58]. However, these syntheses are very sensitive to the slightest changes in reaction conditions, which may affect the quality and reproducibility of the resulting products. They also require the use of inert gas and complex equipment. Therefore, there has been a shift towards implementing syntheses based on green chemistry to provide a straightforward production process and a sustainable alternative to traditional organic syntheses[59]. Most of the reaction solvents (for example, water and ionic liquids), reductants (such as vitamin C) and capping ligands (for example, biomolecules and plant extract) used are water-soluble, naturally occurring and safe[60,61]. For instance, IONPs can be made directly by mixing iron salts in the presence of dextran, a natural polysaccharide, and subsequently raising the pH via the addition of ammonia[62]. Bismuth–iron oxide nanohybrids and cerium oxide NPs can also be synthesized following similar co-precipitation procedures[63,64]. Another example of green synthesis involves the use of natural templates, such as DNA aptamers and viral proteins, to facilitate the assembly of inorganic nanocrystals[65].

**Lipid-based nanomaterials.—**Lipids are amphiphilic molecules that contain a hydrophilic head group and a hydrophobic tail group. Depending on the relative sizes of these groups, lipids can self-assemble into a liposomal bilayer surrounding an aqueous core or a micellar monolayer (or an emulsion) surrounding a hydrophobic core. A standard protocol for forming liposomes comprises mixing of two or more types of phospholipids that usually possess two hydrocarbon chains, such as distearoylphosphatidylcholine and 1,2-distearoylsn-glycero-3-phosphoethanolamine-PEG (DSPE-PEG), with cholesterol (to promote formulation stability) in chloroform, thin film formation, followed by sonication and solubilization in an aqueous medium[66]. By contrast, micelles are formed using a proportion of phospholipids with a larger head group than its hydrophobic component. There are several preparation methods for micelles, including oil-in-water emulsion, solvent evaporation and lyophilization[13]. Passive encapsulation of and lipidic labelling with contrast-generating substances are the common methodologies for formulating liposomal, emulsion and micellar NP contrast agents[67,68]. Examples include the encapsulation of hydrophobic payloads, such as hydrocarbon-coated nanocrystals, fluorophores or

perfluorocarbons (liquid or gas), as well as use of gadolinium chelate or fluorophore-modified lipids. A few formulations, such as liposomes, require post-preparation downsizing to decrease size and dispersity. Techniques such as extrusion, ultrasonication, field-flow fractionation and centrifugation are available for reducing NPs to smaller size ranges.

Biologically derived structures, such as lipoproteins and cell membranes, are naturally occurring nanomaterials that can be repurposed as contrast delivery platforms[69]. There are different types of lipoproteins, such as high-density lipoproteins (HDLs) and low-density lipoproteins (LDLs), but they all have a similar basic structure — a hydrophobic core of triglycerides and cholesterol that is covered with an apolipoprotein containing phospholipid layer[70,71]. Lipoproteins can therefore be considered a form of micelle or nanoemulsion. In general, lipoproteins are extracted from blood serum via ultracentrifugation with increasing densities of potassium bromide solution. HDLs and LDLs are generally in the size range of 7–13 and 22–27 nm, respectively. Moreover, contrast-generating materials can be loaded in the hydrophobic core of lipoproteins[72], for instance, by replacing triglycerides and cholesterol ester with nanocrystals. Contrast-generating materials can also be included in the lipid coating by attaching contrasting elements to the protein constituent or by incorporating contrast-labelled amphiphiles in the formulation[73].

An alternative approach for the assembly of lipid-like NPs is in vivo self-assembly. In a recent example, monomers containing an FDA-approved drug, olsalazine, were dimerized in situ via a reaction catalysed by the enzyme furin, which is overexpressed in colon tumours[74]. The dimer aggregates into NPs, which can be detected via CEST or Raman imaging, and has anti-cancer effects, all of which arises from the olsalazine component[75].

**Polymeric nanoparticles.—**Polymeric nanomaterial-based contrast agents are typically composed of natural polymers (for example, dextran and chitosan) and synthetic polymers (for example, polyethy-lenimine and poly(lactic-co-glycolic acid)), which are further divided into multiple subclasses, such as polymersomes and dendrimers. Conventional polymeric NPs are typically synthesized via covalent conjugation, cross-linking or physical encapsulation[76]. Single or multiple contrast agents can be encapsulated within the carrier matrix to enable multimodality imaging. Furthermore, some polymer matrices may provide intrinsic contrast, such as semiconducting polymers with PA and NIR fluorescence imaging capabilities[77,78]. Such polymers can self-assemble into NPs by interacting via the hydrophobic effect. Finally, a microfluidic chip could be used to crosslink water-soluble polymers with hydrophilic contrast cargoes via ionic interactions[79].

Dendrimers (for example, poly-L-lysine and polyamidoamine (PAMAM)) are highly branched, tree-like nanostructures that result from a sequence of reaction steps using divergent or convergent methods[80]. Each step leads to an additional generation of branching as well as an increase in the number of available surface functional groups. Therefore, generation 5 PAMAM dendrimers display more primary amino groups compared with previous generations, allowing for incorporation of targeting ligands in addition to contrast agents[81]. For instance, generation 5 PAMAM dendrimers were used to entrap 2 nm AuNPs inside PEG cavities as well as attach Fluo-4 via covalent conjugation for labelling T cells and thereby imaging and sensing their location and activity[82].

## Nanoparticle modification and conjugation

For use in biological settings, toxic surfactants and hydrophobic ligands need to be displaced to render colloidal nanocrystals hydrophilic with good stability and biocompatibility. Approaches to this include direct ligand exchange, embedding in a carrier matrix (for example, silica and polymer) or coating with amphiphilic molecules (for example, micelles and vesicles) (Fig. 2b). For example, citrate ions act as a capping agent for gold nanocrystals and are typically substituted with thiolated compounds, such as thiol-PEG or glutathione, through direct incubation owing to the strong affinity of sulfur with gold[83]. However, post-synthesis modification via transfer to the aqueous phase can be quite cumbersome and may affect certain NP characteristics (such as pharmacokinetics) that are highly dependent on the surface structure.

Surface functionalization with targeting moieties, cargoes and chelators can be achieved using several established methods[84–86] (Fig. 2c). One commonly utilized strategy is the *N*-ethyl-*N*´-(3-dimethylaminopropyl)carbodiimide/*N*-hydroxysuccinimide-mediated carboxylate–amine coupling. More recently, click chemistry via copper-catalysed azide–alkyne cycloaddition is a preferred bioconjugation method[87]. Click chemistry is most suited for the conjugation of targeting ligands to NPs as it forms highly oriented linkages and ensures site-specific binding. However, as most biomolecules and NP surfaces do not normally contain azide and alkyne groups, pre-activation is required to carry out the reaction, which can increase the complexity of the work. Bioconjugation can also be achieved by using an intermediate crosslinker, such as bissulfosuccinimidyl suberate and sulfosuccinimidyl 4-(*N*-maleimidomethyl)cyclohexane-1-carboxylate, to facilitate linkage between two complementary or different functional groups[88]. In addition, the specific and stable interaction between streptavidin and biotin, which is less likely to alter or interfere with the biomolecule activity, can be used. Nevertheless, several factors, such as cost, effectiveness, NP stability and bioactivity change associated with each method, should be taken into consideration when choosing a bioconjugation strategy that is most suitable for the NP–biomolecule pair.

## Nanoparticle purification

The high density of many NPs allows unreacted molecules or unconjugated moieties to be easily removed via repeated centrifugation, thus producing a highly concentrated and purified product. Density gradient centrifugation via potassium bromide or sucrose is used when the density difference between the product and by-products is low, such as LDL loaded with 3 nm AuNPs[89]. Another purification method involves the use of molecular weight cut-off (MWCO) concentrator tubes, which separate impurities and NPs into different compartments via centrifugation based on the relative sizes. In a related approach, MWCO dialysis membranes or ultrafiltration columns are used together with a large volume of fresh buffer to allow free ions to diffuse into the reservoir over time. The NP products are retained by the MWCO filters given the appropriate pore size (for example, 10 kDa MWCO for 15 nm AuNPs). Finally, NPs can be precipitated using an incompatible or insoluble solvent and washed using a solvent in which the impurities are soluble (Fig. 2d).

# Results

Nanomaterial designs can vary widely in size, shape and composition, among other physicochemical properties. It is generally accepted that these factors strongly influence the contrast and bio-interactions of nano-based agents. In this section, analytical characterization methods used to identify the physical and chemical features of various nanomaterial types are discussed[90]. Although each technique has its own advantages and use cases, a combination of multiple techniques is essential to provide conclusive nanomaterial characterization, as well as information related to cellular specificity and in vivo fate and performance of nano-based contrast agents. Imaging approaches that can be used to assess the behaviour of the agent in vitro and in vivo are also described. Finally, how these properties define the suitability of an NP for different imaging applications and alter its interactions at the nano–bio interface is examined.

## Physicochemical characterization

**Size and morphology.—**In nanomedicine research, the results section typically begins with NP characterization data. Size and morphology are key characteristics that can affect contrast generation, pharmacokinetics, biodistribution and other agent properties. Synthesis and characterization often occur in a feedback loop, in which results from characterization are used to inform changes to synthetic conditions in an effort to generate NPs that meet design criteria or have high performance. Micrographs from transmission electron microscopy (TEM) and scanning electron microscopy (SEM) show the NP core (Fig. 3a) and surface morphology, respectively[91]. NP shape or geometry can be easily visualized by both techniques. High-resolution TEM is sometimes performed to characterize the lattice fringes of nanocrystals. Freeze-fracture TEM can be used to study the structure of NPs made of soft materials such as lipids or proteins. NP surface topography can be assessed by atomic force microscopy[92]. Moreover, dynamic light scattering (DLS) is the main method to determine the hydrodynamic diameter ($D_h$) and size distribution of NPs in suspension[91] (Fig. 3b), although it should be noted that DLS typically assumes spherical morphology; therefore, it is less informative for non-spherical agents[93,94]. A homogeneous NP size distribution contributes to consistent in vivo behaviour; therefore, the NP size range, or the polydispersity index (PDI), should be noted. A PDI value of <0.1 typically indicates a properly monodisperse NP population, whereas larger PDI values are acceptable under certain circumstances, for example, NPs produced from complex multistep syntheses. NP tracking analysis (NTA) and fluorescence correlation spectroscopy are also useful tools for measuring the size and number of NPs in solution, respectively[94–96]. For certain formulations, the porosity of NPs is examined via focused ion beam tomography in conjunction with electron microscopy[97].

**Chemical composition.—**The elemental composition of NPs can be assessed using several techniques such as inductively coupled plasma (ICP) spectroscopy, energy-dispersive X-ray spectroscopy, X-ray diffraction and X-ray photoelectron spectroscopy. ICP is frequently used to measure the concentration of metal elements in samples, which is particularly relevant given that metals are commonly present in NP contrast agents. Energy-dispersive X-ray spectroscopy identifies the presence of certain elements in a sample

by analysing the emitted characteristic X-rays[5] (Fig. 3c). X-ray diffraction examines the crystallinity and lattice planes of dried NPs by recording the diffraction patterns of scattered X-rays. X-ray photoelectron spectroscopy operates on the basis of the principle of photoelectric effect to determine the core and surface elemental composition, as well as the binding or oxidation states of the elements[98]. Other methods can be used, depending on the NP composition. For formulations that contain phosphate groups, for example, phospholipid-based NPs, colorimetric assays can be used to assess the amount of inorganic phosphate and thus to determine the final phospholipid inclusion[99]. The protein content of NPs can be measured by the Bradford assay, for example. Such methods are important for understanding the degree of conjugation success or composition-contrast generation relationships.

**Surface chemistry.**—Characterization of NP surface chemistry is important as the surface has direct exposure to biological components, which can affect the overall NP stability, toxicity and functionality. The net surface charge of NPs is presented as zeta potential, which can vary widely with the solvent type and pH of the solution. High surface charge increases repulsive forces between NPs, thus improving the colloidal stability and promoting interactions with oppositely charged molecules of interest[100]. Fourier transform infrared spectroscopy is the main technique for identifying functional groups or surface ligands and for detecting changes in surface properties. Nuclear magnetic resonance (NMR) can also be used for this purpose; however, various effects from the attachment of ligands to NP surfaces (for example, superparamagnetism of IONPs or decreased ligand rotation from surface immobilization) can render NMR data hard to obtain or interpret. Nevertheless, for some types of NPs, NMR can yield key insights into surface chemistry[50]. Thermogravimetric analysis can be used to quantify the density of targeting moieties, or the number of organic ligands present on the NP surface.

**Stability.**—Stability should also be assessed for weeks to months after synthesis, depending on the storage conditions and suspension fluids, to determine the shelf-life and ideal time frame (absence of aggregation) for performing subsequent studies. Nano-based contrast agents are incubated in simulated biological fluids, such as phosphate-buffered saline with 10% fetal bovine serum, to assess their stability under physiological conditions. NTA, DLS, UV–Vis measurements and asymmetrical field-flow fractionation are used to evaluate changes owing to agglomeration and formation of protein corona[101]. Formulation stability can also be examined via the release of payloads or metal ions owing to degradation or leaching. This can be assessed using ICP and the aforementioned analytical techniques.

### Contrast properties

NPs can be used as contrast agents based either on their inherent contrast properties or on functionalization with contrast-generating moieties. To characterize the contrast properties, a series of increasing concentrations of the contrast agent together with relevant controls, such as water, saline, air and comparator agents (for example, FDA or EMA-approved agents such as Gd-chelates for MRI and iodinated molecules for CT), are inserted into a phantom, which is a device composed of tissue-equivalent materials and can be scanned to evaluate the imaging performance of agents. The qualities desired for these phantoms

vary by scanner type and their designs range from simple to complex (phantoms used for CT include a bucket of water to 3D-printed chest mimics), with the goal that more complex phantoms will be a better predictor of in vivo contrast generation, result in better image quality or otherwise provide advantages[102–105]. The phantom is then scanned with the desired imaging instrument using a set (or multiple sets) of acquisition parameters. Contrast properties of the NP formulation of interest should be measured within the linear portion of the standard curve. A broad range of concentrations should be tested to determine the optimal dose for in vivo administration as NPs are expected to accumulate in various organs at differing concentrations. The doses needed for in vivo studies may be estimated from previous, similar experiments, although some trial and error (such as dose optimization) may be needed for any new agent. Depending on the imaging application, specialized devices may be used to characterize signal output in vitro. Finally, quantification of in vivo contrast enhancement is generally performed via advanced image analysis software, such as ImageJ and MATLAB. Regions of interest are drawn over certain features (such as tumours), and results are typically presented as contrast-to-noise ratio or tissue-to-background ratio. Artificial intelligence methods for both image reconstruction and image analysis have drawn considerable attention recently and may have a larger role in the future[106,107].

**X-ray imaging.**—CT phantoms can be constructed simply by securing vials of NP samples in plastic racks and submerging in water to simulate beam hardening, or the rise in average energy of an X-ray beam as it is attenuated by the body[108]. Anthropomorphic phantoms can also be utilized, such as chest phantoms that mimic the human organs in the thorax, in terms of thickness, density and mass attenuation[105]. Furthermore, phantoms for mammography are fabricated using varying compositions of glandular and adipose tissue equivalent materials[109]. These phantoms are scanned using a range of X-ray tube voltages, beam filters, current, slice thickness, exposure time and field of view. CT attenuation, as displayed in Hounsfield units (HU), increases linearly with NP concentration[110] (Fig. 3d). The slope of the linear regression line, or attenuation rate ($HU \cdot ml \cdot mg^{-1}$), is then calculated to characterize CT contrast. Mammo-graphic contrast is shown as contrast-to-noise ratio or signal difference-to-noise ratio by measuring signal intensity from the sample (or tissue of interest) and background (for example, body of the phantom).

**MRI.**—MRI phantoms can be prepared by inserting NP samples in an agarose gel doped with manganese, nickel or other salts[63,111]. Depending on the mode of detection, the phantom is scanned using $T_1$-weighted or $T_2$-weighted sequences at multiple echo times, repetition times or inversion times[112] (Fig. 3e). Signal intensity is measured at each echo time and inversion time for the determination of $T_2$ and $T_1$ relaxation times, respectively; $r_1$ and $r_2$ relaxivities can then be calculated through curve fitting of the inverse of $T_1$ and $T_2$ relaxation times as a function of NP concentration. Alternatively, relaxivity measurements can be performed with a benchtop device known as a relaxometer. For in vivo MR contrast measurement, pixel-wise curve fitting of the relaxation times can be used to generate colour-coded maps of $R_1$ and $R_2$ relaxation rates. The contrast generation of $^{19}F$ MRI agents can similarly be assessed by measurements of $r_1$ and $r_2$ using NMR spectrometers or other systems[113]. Alternatively, samples can be scanned at a range of concentrations and the SNR analysed[114]. The contrast generated by CEST agents can be assessed using sets of MR pulse

sequences to determine the ppm shift from water where the maximum chemical exchange is observed[115]. Water exchange rates are also determined.

**Nuclear imaging.**—PET radioisotopes are often produced in a cyclotron using nuclear reaction processes, with a specific activity at the end of bombardment. Radionuclides can be attached to the NP surface or interior using chelator-based or chelator-free labelling methods[116]. Radiolabelled NPs can usually be purified by size exclusion column chromatography with phosphate-buffered saline as the mobile phase. Radiolabelling yield can be determined by direct radioactivity measurement or by using an autoradiograph of a thin layer chromatography plate with EDTA as the mobile phase[117]. Radiolabelling stability is usually evaluated after incubation with serum at various time points. Before animal studies, radioactivity of a sample is assessed using a well counter to calculate the injection dose needed for adequate detection in vivo. Regions of interest are drawn on PET images to measure biodistribution in vivo, whereas the major organs and tissues are often collected to quantify biodistribution ex vivo using a $\gamma$-counter[118]. Finally, owing to the high detection sensitivity of nuclear imaging, low labelling densities are required in comparison to the high labelling required for MRI-active NPs, for example.

**Fluorescence imaging.**—The signal generation of fluorescent NPs should be evaluated in tissue-mimicking phantoms with defined light scattering properties to nullify issues related to fluorescence (self) quenching and light absorption in biological tissues. Assessments can be done with the scanner intended for in vivo use, as well as fluorometers. Combinations of excitation and emission wavelength pairs should be tested to determine optimal imaging parameters. Fluorescence intensity usually exhibits a non-linear relationship with NP concentration, so a broad range of concentrations should be tested to identify the detection saturation threshold. The effects of target depth can be assessed by including differing thicknesses of tissue-mimicking materials in the phantom between the samples and the scanner optics.

**Photoacoustic and ultrasound imaging.**—PA phantoms can be created by mounting tubes of NP samples into a plastic holder that is immersed in deionized water free of air bubbles[119]. More complex phantom designs can be created from moulded plastics, for example, in which depth penetration can be explored with phantoms of varying thicknesses[120]. The transducer is placed above the phantom (in contact with the water or using ultrasound gel to provide contact with plastic phantoms), and PA signals are acquired using an NIR excitation wavelength with a defined PA gain. PA spectra (intensity versus wavelength) are collected to characterize NP signal generation within the NIR range and to determine optimal imaging conditions. Integrated pixel density of the diseased region before and after injection can be quantified to show PA contrast enhancement. Ultrasound agent assessment can be done with similar physical set-ups to PAs. Samples are tested over a range of concentrations and frequencies. Dedicated sample testing systems can be used, as well as preclinical or clinical systems[121].

## Biological characterization

**In vitro studies.—**To examine cytotoxic effects, primary cells and/or cell lines of interest are treated with NPs at a range of concentrations, and cell viability is analysed using various assays, such as MTS and LIVE/DEAD staining. Two-dimensional cell cultures are commonly reported for this purpose; however, more sophisticated in vitro models, such as organoids and organ-on-a-chip, more closely mimic disease pathophysiology and local microenvironments[122]. This allows for better prediction of in vivo NP cytotoxicity and imaging and treatment efficacy. More detailed examination of the effects of NP contrast agents on cells in vitro can be performed to better understand their potential toxicities. For example, NP surface reactivity can be investigated by the ferric reduction of serum assay or intracellular oxidative stress (Fig. 3f) assays, such as DCFH-DA and TBARS[5]. Should toxicities arise, such assays can inform on methods that can be used to reformulate to avoid toxicity, such as changing surface ligand or polymer molecular weight.

For targeted imaging applications, it is important to evaluate the affinity and specificity of targeted NP contrast agents for their intended targets. Receptor binding assays should be conducted to demonstrate the ligand specificity. Cells are pre-treated with free variants of the targeting ligand (or receptor blocker), followed by targeted nano-based contrast agents, a method known as competitive inhibition. Additional methods to test cell-specific NP targeting include incubating the cells of interest with NPs that have varying amounts of the targeting ligand at low and high temperatures to inform on uptake mechanisms, as well as under static and flow conditions to provide insights on which tissues will have greater uptake. Assessment of cellular uptake of nanomaterials could be performed via techniques such as fluorescence microscopy (Fig. 3g), SEM and TEM (Fig. 3h), flow cytometry or contrast quantification (for example, $\gamma$-counting or CT attenuation of cell pellets)[123,124]. NPs can be taken up by the cell via different endocytic pathways. Blocking of these pathways using inhibitors or cells with genetic knockouts can reveal the contribution of each endocytic pathway in the uptake process and determine the ability of NPs to undergo endosomal escape.

**Preclinical in vivo studies.—**Appropriate animal models, in terms of species, age and gender, should be selected for each disease application[90]. A power analysis is then performed to calculate the number of animals required for each cohort. Many imaging studies use on average five to seven animals per treatment group. For most applications, intravenous injection is the standard route for nanomaterial administration. Depending on the specific imaging purpose, other injection methods can be used, such as interstitial and orotracheal administration for mapping of sentinel lymph node and lung activity, respectively. Furthermore, NPs can be monitored at defined time points post injection (minutes to weeks) to estimate their circulation time and tissue uptake. Nuclear imaging (using radiolabelled NPs) is the best technique for evaluating pharmacokinetic and biodistribution profiles owing to its high detection sensitivity (Fig. 3i) and ability to longitudinally image any depth in the patient[125]. The elimination route of NPs can be easily determined by analysing faecal (via hepatobiliary system) and urine (via renal system) samples after injection. The amount of NPs found at the target site should be presented as

percentage of injected dose per gram of tissue (%ID $g^{-1}$) to normalize data reporting for more direct comparison.

Nano-based contrast agents should be thoroughly assessed for their in vivo biocompatibility. Typically, multiples of the intended dose of NPs are injected in healthy cohorts, and the animals are monitored regularly over a long period of time. Blood samples are drawn and analysed to detect biomarkers that are indicative of potential inflammatory responses as well as damages to liver (ALT and AST) and kidney (BUN) functions[64] (Fig. 3j). Routine welfare checks are performed to identify changes to the overall physical and mental health (for example, body weight, behaviour and signs of weakness) of the animals. Upon euthanization, major organs are collected and subjected to extensive histological analyses to detect any phenotypic changes.

## Applications

Nano-based contrast agents have been demonstrated to visualize various pathologies and gain insight into underlying disease mechanisms through structural and functional imaging. Some multimodal NP diagnostics have been developed to possess additional therapeutic functions, which are also known as theranostics. In this section, representative applications of nano-based contrast agents in several key areas of medical imaging research are presented, and nano-based contrast agents that are approved or currently under clinical evaluation are discussed.

### X-ray nanomaterials

Delineation of the vasculature has become a major application of CT[126]. These agents are typically large ($D_h > 10$ nm) with bulky surface ligands to bypass renal clearance[8]. The most frequently reported CT blood pool agents are PEGylated AuNPs and iodine-loaded liposomes or nanoemulsions[127–129]. Moreover, iohexol, an approved iodinated molecule, was crosslinked with a homopolymer to improve blood circulation and to enhance tumour contrast owing to passive accumulation via the EPR effect[130]. Similar findings have been reported for breast cancer imaging with DEM using PEGylated gold–silver alloy NPs, PEGylated silver telluride NPs (PEG-$Ag_2Te$) and micelle-encapsulated $Ag_2S$ NPs[131–133]. Notably, PEG-$Ag_2Te$ has been found to produce stronger X-ray contrast compared with elemental silver NPs owing to the inclusion of tellurium. In addition to imaging the blood pool and tumours, CT in conjunction with metal (such as gold and cerium) NPs has increasingly been utilized for detecting inflammatory diseases, such as colitis and abdominal aortic aneurysms[23,134]. Several studies have also shown the feasibility of quantifying inflammatory macrophage content in atherosclerotic plaques via spectral CT (capable of resolving individual photon and classifying them into energy bins to produce quantitative elemental maps) with gold cores in PEG coating or HDL[135,136] (Fig. 4).

With rapid development in cell-based therapies, the topic of cell tracking with CT has garnered considerable interest, although high contrast payloads are needed to overcome the low sensitivity of CT, such as >10 pg per cell[1,137]. Many nano-based CT contrast agents have been engineered to facilitate uptake by various cell types, such as stem cells and immune cells[138–140]. For example, it was demonstrated that CT contrast is linearly

proportional to the number of AuNP-labelled mesenchymal stem cells, highlighting the quantitative nature of CT imaging[141]. Furthermore, AuNPs with various sizes and coatings were examined with CT scans for optimal uptake by monocytes. It was found that 50 and 75 nm AuNPs with carboxylic acid ligands provided the most internalization[142]. Note that inherent CT contrast generation is dependent on elemental mass concentration but independent of NP size[52].

Several high $Z$ elements, specifically those that make potent CT agents, can induce DNA damage and cell death through radio-sensitization. For example, RGD-targeted AuNPs can augment radiotherapy by delivering radiation dose preferentially to endothelial cells of tumour neovessels[143]. PEGylated bismuth NPs can also induce antitumour effects by allowing CT image-guided radiotherapy and photothermal therapy (PTT)[144]. Finally, advances are being made to develop novel CT agents that generate the most optimal contrast, such as ytterbium and tantalum NPs, which can be further utilized for multiplexed imaging with spectral CT[110,145–147].

### Magnetic nanomaterials

Most magnetic nanomaterials reported to date are based on gadolinium or iron[148–150]. Gadolinium is paramagnetic and such agents provide excellent $T_1$ contrast and are frequently based on chelated gadolinium ions. For instance, HDL NPs were labelled with gadolinium chelates and conjugated with a collagen targeting peptide to monitor the compositional changes in atherosclerotic plaque regression via MRI[151]. Interestingly, poly-L-lysine-coated $NaGdF_4$ nanodots were synthesized, resulting in a dual-modality contrast agent that is capable of anatomical and functional imaging[152]. These nanodots possess high longitudinal relaxivity for $T_1$-weighted MRI and also exhibit an excellent CEST effect for pH mapping of brain tumours. However, free gadolinium can deposit in the brain with unknown long-term effects and can also induce nephrotoxicity in patients with renal disease. Other $T_1$ agents, such as MnO NPs, have been developed with the hypothesis that they will offer better patient safety[153,154]. For example, hollow MnO NPs with expanded water-accessible surface areas were used for transplant tracking and drug delivery in addition to enhanced $T_1$ MRI[155,156]. Such manganese-based NPs can yield $T_2$ or dual-mode $T_1/T_2$ contrast through appropriate size control[157].

IONPs are superparamagnetic and are the most studied $T_2$-shortening contrast agent[158,159]. They have been used for MR detection of cancer and atherosclerosis, imaging of circulating cells and tracking of labelled stem and immune cells[160–162]. In the clinical setting, dextran-coated ultrasmall superparamagnetic IONPs have been used to target intraplaque macrophages to evaluate the efficacy of novel cardio-vascular therapeutics[163]. As a preclinical example, the M13 filamentous bacteriophage template with a glycoprotein targeting peptide was used to assemble IONPs for improved MRI of prostate cancer[164]. In another study, two complementary IONPs (6 nm) were designed to self-assemble into larger nanoclusters (800 nm) and boost $T_2$ relaxivity after undergoing a biorthogonal reaction when cleaved by tumour enzymes[165]. Notably, IONPs can transition into a $T_1$ contrast agent by decreasing their size. $T_2$ effects can also be increased by doping IONPs with transition metals, such as manganese, or by forming alloys with other metals (such as FeCo)[166]. In

addition to their MRI applications, IONPs can be utilized to track stem cells via MPI, an emerging technique that exploits nonlinear magnetization of NPs to generate positive contrast images[167]. Notably, FeCo NPs have recently been shown to improve the detection sensitivity of MPI owing to higher magnetic saturation[168].

### Radiolabelled nanomaterials

Nanomaterials have traditionally been labelled with radionuclides through coordination chemistry using exogenous chelators. DOTA, NOTA (or their derivatives) and deferoxamine (DFO) are the commonly used chelating agents for complexation of $^{64}Cu$ and $^{89}Zr$ radioisotopes, respectively[169]. These chelators are conjugated to the NP surface to facilitate disease detection and cell tracking via PET[170–173]. For instance, polymeric dextran NPs or HDL NPs were labelled with DFO for $^{89}Zr$ chelation and were used to detect resident macrophages in assessing atherosclerotic plaque inflammation via PET imaging[174,175]. Moreover, selenium-doped carbon QDs with reactive oxygen species (ROS) scavenging properties were labelled with $^{89}Zr$ via DFO and demonstrated superior efficacy in the treatment of acute kidney injury[125]. Their uptake in the kidneys was quantitatively measured by PET imaging. Similar chelation strategies have been implemented for radiolabelling nanomaterials for SPECT[176]. For example, $^{99m}Tc$-labelled nanostructured lipid carriers were found to specifically target brown fat tissue via SPECT, which may prove beneficial for imaging metabolic disorders in humans[177]. Interestingly, NOTA, which has better stability compared with DOTA[178], can chelate $^{64}Cu$ and be further conjugated onto RGD-functionalized superparamagnetic IONPs for targeted imaging of tumour neovessels via PET and MRI[179]. Antibody-conjugated mesoporous silica NPs and unimolecular micelles that carry chemotherapeutics can also be radiolabelled in a similar fashion to enable targeted tumour imaging and drug delivery[180–182].

Chelator-free, intrinsic radiolabelling has recently been extensively investigated as an alternative to traditional chelation techniques. Several synthetic methods, such as hot-plus-cold precursors, specific trapping and cation exchange, can be used to acquire intrinsically labelled nanomaterials[183]. The hot-plus-cold precursors approach, such as integrating $^{64}Cu$ into CuS NP cores, has led to a multifunctional agent with PET imaging and PTT capabilities[184,185]. Other radioactive metal ions, such as $^{89}Zr$ and $^{69}Ge$, have displayed strong binding affinity towards metal oxide NPs with high labelling yield and good serum stability[186,187]. For instance, $^{69}Ge$-labelled superparamagnetic IONPs were synthesized by simple mixing and used for lymph node mapping via PET and MRI[188] (Fig. 5). In another example, $^{64}Cu^{2+}$ ions were adsorbed onto $MoS_2$ nanosheets without chelating molecules owing to the affinity between copper and sulfur at molybdenum defect sites[189,190]. This post-synthesis labelling approach yielded a theranostic nanoplatform that provides PET and PAI-guided tumour ablation.

### Optical nanomaterials

Metal-based semiconducting QDs with narrow band gaps are perhaps the most sought-after nanomaterials for fluorescence imaging applications[191,192]. By modulating the reaction time and solvent, the core diameter of $Ag_2S$ QDs was tuned from 1.5 to 9 nm, which corresponded to an emission wavelength from 500 to 1,200 nm, allowing for detection in the

NIR-I and NIR-II regions[193]. Furthermore, RGD-conjugated, NIR-emitting, mercury QDs with a membrane impermeable etchant can be quenched in excess via cation exchange, thus achieving tumour-specific fluorescence imaging with high sensitivity[194]. However, many QDs contain heavy metals, such as mercury or cadmium, which are strongly toxic at low concentrations and may therefore cause safety issues that hinder their clinical translation.

Carbon QDs, an organic nanomaterial with minimal toxicity, can be synthesized to display semiconductor band-gap-like fluorescence via surface passivation-induced defects[195]. For instance, carbon QDs with surface doping of zinc sulfide have similar quantum yield compared with well-established CdSe QDs[195]. Other carbon-based nanomaterials, such as graphene, nanodiamonds and nanotubes, possess exceptional optical properties in the NIR-II window, where relatively deep tissues (for example, brain microcapillaries and lung stem cells) can be visualized[196–198]. NIR-II fluorescence imaging is also useful in detecting brain vasculature and blood flow with fluorophore-conjugated polymeric NPs and rare-earth downconverting nanocrystals[199,200].

Gold nanomaterials also have use in fluorescence and other optical imaging applications. NIR fluorescent gold nanoclusters (AuNCs) were encapsulated in red blood cell membranes to improve blood circulation for enhanced tumour accumulation and contrast[201]. Targeted kidney imaging has been achieved using AuNCs-loaded ferritin nanocages[202]. Moreover, surface plasmon resonance (SPR) in metallic nanostructures (gold, silver and copper) can induce SERS effects for Raman imaging[203,204]. For example, colon cancer detection was performed using silica-coated SERS AuNPs with a dedicated Raman-based endoscope[205]. SERS-enhanced gold nanostars were synthesized to support surgical resection with Raman-assisted guidance to ensure complete tumour removal[206]. In addition, the amount of metallic nanomaterials needed for clinical SERS imaging can be greatly reduced by embedding additional Raman dyes in the surface coating[207]. It is worth noting that, unlike any other biomedical imaging modalities, nano-based SERS imaging is capable of profiling molecular targets with highly multiplexed capabilities[208].

## Photoacoustic nanomaterials

Gold nanostructures are a class of contrast agents with appealing PAI properties, owing to their tunable SPR peaks via size and geometric modifications[209,210]. For instance, sub-5-nm AuNPs were encapsulated in larger biodegradable polymeric nanospheres, which provided significant PA contrast enhancement in vivo owing to a red shift in their absorption from interparticle plasmon coupling[79]. AuNPs-loaded ROS responsive polymeric nanospheres provided differential PA contrast (signal loss) in ROS-rich microenvironments, such as inflammation and cancer[211]. The presence of ultrasmall AuNPs makes them a dual-modality PA and CT contrast agent with the potential for swift renal elimination upon degradation. Polymeric NPs can also carry and deliver therapeutic drugs via PAI guidance[212]. In addition, AuNPs conjugated with epidermal growth factor receptor (EGFR) antibodies and coated with NIR-active molecules allowed for targeted tumour imaging with bimodal PAI and SERS imaging[213]. Furthermore, a new class of PA contrast agents based on NIR-absorbing semiconducting polymers has been introduced[214,215]. A study showed that ROS levels can

be measured by quantifying PA signals from ROS-sensitive dye-decorated semiconducting polymeric NPs at different input laser wavelengths[77].

Other nanomaterials apart from AuNPs also make potent PA contrast agents[216]. AuNRs have been extensively applied in PAI owing to tunable transverse and longitudinal SPR peaks that can shift into the NIR region[118]. It was reported that miniature AuNRs can significantly enhance PA contrast in tumour compared with larger AuNRs, indicating a size effect on PA signal generation[217]. PAI can also be used for tracking and quantifying mesenchymal stem cell in rodent muscle tissue with silica-coated AuNRs[218]. Similarly, $Ag_2S$ NPs (Fig. 6) and $TiS_2$ nanosheets exhibit intense NIR light absorption and are excellent for theranostic applications through PAI (and NIR fluorescence imaging) and PTT[219,220]. Finally, an unconventional class of PAI agents, which is based on upconversion nanomaterials, has recently emerged[221]. $NaYF_4$ upconverting NPs doped with lanthanide ions and complexed with α-cyclodextrin showed remarkable PA signal enhancement in vivo owing to luminescence quenching from non-radiative relaxation.

## Reproducibility and data deposition

The condition sensitivity of nanomaterial synthesis and nano–bio interactions can affect data reliability and reproducibility, leading to variability in experimental findings. Moreover, inconsistent results at the preclinical stages may present challenges for clinical translation. To address such issues, the nanomedicine community has proposed to adopt the minimum information reporting in bio–nano experimental literature (MIRIBEL) guidelines for standardizing data reporting[222–224]. This section describes best practices for producing high-quality, reproducible results and discusses potential repositories for accessing experimental data related to nano-based contrast agents research.

For some nanomaterial types, the synthetic process can be quite extensive and may involve multiple reagents and complicated preparation protocols. To minimize batch-to-batch variations, it is important to provide detailed synthesis and purification procedures and note any sensitive or challenging operations[225]. Photographs showing the experimental set-up, each successive reaction step and appearance of the final products could be included to allow for more accurate synthesis replication. Reagent information such as manufacturer, lot number, expiration date, storage requirement, stability and purity could be listed, as well as quality acceptance criteria[226].

Rigorous reporting of NP characterization data is crucial for improving data reproducibility. According to the MIRIBEL guidelines, physicochemical properties including the size, morphology, dispersity and zeta potential should be reported as a minimum. Readouts on three or more individually produced NP batches should be included to inform the robustness of the synthesis and reproducibility of the product. Measurements should also be conducted in biologically relevant media as changes may occur owing to aggregation. More than two independent characterization methods should be utilized to fully understand the material properties of an NP contrast agent with a detailed description of how a parameter is assessed. This includes sample preparation steps, controls, equipment information, instrument calibration procedures, acquisition protocols and analysis software version. It

is essential to provide a distribution (or a range) of the measured parameter instead of a single average value. NP contrast properties should be investigated using well-constructed, contrast-embedded phantoms, and details of phantom design and image reconstruction and analysis should be provided. For in vivo imaging experiments, information detailing the animal strain, disease model, administration route, injected dose and volume, injection rate, NP suspension buffer and image processing methods (for example, thresholding) should be documented. Finally, researchers should make use of self-checklists, validated assays and standard operating procedures to ensure accurate and reproducible outcomes.

As recommended by the MIRIBEL guidelines, it would be beneficial if raw data and experimental reports were provided together with manuscript submission or deposited in online open-access repositories. Funding bodies such as the NIH are placing a greater emphasis on scientific data sharing. However, the development of large-scale, trusted data repositories for nanomaterial and medical imaging research is still at its inception. Thus, researchers should take advantage of currently available data sharing platforms such as GitHub and preprints (for example, ChemRxiv) to promote early data exchange and to facilitate timely communication. Further experimental details, results and statistical analyses should be included in the supplementary information to improve transparency. Finally, dedicated journals that outline specific synthetic protocols, characterization techniques and imaging methods may ensure thorough evaluation of published studies and establish successful standardization practices[227].

## Limitations and optimizations

Even though nano-based agents have great potential to provide rich imaging contrast, certain design elements should be considered and further optimized before their clinical implementation. This includes ensuring reproducible and cost-effective NP synthesis in large scale, maximizing their imaging sensitivity, resolving biocompatibility and toxicity concerns and enabling effective delivery to target sites.

### Fabrication

As a rule of thumb, simpler synthetic methods generate particles with a wider particle size distribution, which can result in batch-to-batch inconsistencies and may require secondary size selection steps. Fortunately, recent advancements in analytical capabilities, such as TEM and NTA, allow for deeper understanding of nanomaterial properties and easier optimization of synthetic protocols. For inorganic NP fabrication, a two-step process is often involved: NP creation followed by stabilization to prevent aggregation and improve biocompatibility. However, regulatory agencies will typically favour easier one-step aqueous processes, such as the fabrication of liposomes, which are biodegradable and have already been FDA-approved. Dendrimers, in comparison, require a costly multistep process. Preclinical studies investigating new nanomaterials are often not systematically designed or optimized for clinical translation, and most academic laboratories are not equipped with certified good manufacturing practice capacities or the ability to scale up to meet clinical needs. In addition, few commercial manufacturers have previous experience with the synthesis and scale up for biological applications of many of the

types of nanomaterials that are used as contrast agents. As a result, manufacturing and characterization complexities of nano-based imaging agents can lead to poor product reproducibility and reliability[228]. Prioritizing commercialization challenges, assessing manufacturing complexities, considering available scale-up resources and defining rigorous measures for quality control at an early stage of development can increase overall potential for success in clinical translation. To avoid risks of overengineering and fabrication complexity for FDA or EMA approval, careful consideration should be made early on towards pairing the right NP type with the appropriate clinical application.

## Imaging performance

Medical imaging modalities, such as PET, CT, MRI and PAI, that provide anatomical information and visualize cellular and biological processes have potential to transform patient care[205,229,230]. Each of these imaging techniques has its own unique advantages. However, no single imaging modality currently meets all the criteria of high sensitivity, high specificity, high spatial and temporal resolution, high multiplexing capacity, deep tissue penetration, low cost and high throughput. Therefore, considerable efforts have been made to develop multimodal imaging approaches that aim to circumvent the inherent limitations of each modality. Nanomaterials are attractive vehicles for multimodal imaging as they may inherently generate more than one type of contrast or can easily be loaded with multiple forms of contrast in a single platform[131,231–238]. However, a challenge for such multimodal agents is generating detectable contrast for each technique with the same NP dose.

Theranostic NP agents may result in better patient outcomes via simultaneous disease detection and treatment planning. For example, owing to high X-ray attenuation, high light absorption and high plasmon resonance effect, certain designs of AuNPs produce strong CT, PA and Raman contrast, as well as enhance the efficacy of radiation therapy and phototherapy[79,208,239,240]. IONPs induce negative contrast, which may be difficult to identify with certainty. For instance, if the target is expressed in very low concentrations and tissues produce inhomogeneous MR signals, it may not be possible to distinguish the contrast arising from IONPs from the background. Image acquisition sequences that produce positive contrast from IONPs can mitigate this difficulty. As each imaging modality can offer varying ways to quantify image signal intensity, researchers should take care when comparing and interpreting their data across the field, particularly when optimizing nano-based contrast agents for improved detection sensitivity.

## Toxicity

To achieve eventual clinical approval, nano-based contrast agents are subjected to thorough assessments of their long-term biodistribution, degradability, clearance and toxicity. Lipid-based and silica-based NPs have shown to be biodegradable in the body, but there are concerns about the biocompatibility and stability of many inorganic NPs, with a few exceptions such as iron oxides and manganese oxides, which are generally regarded as reasonably biodegradable and biocompatible[241,242]. QDs often contain heavy metals, such as cadmium and lead, that are strongly toxic at low concentrations[243]. Thus, QDs that have biocompatible coatings or are free of heavy metals are more likely be considered for eventual clinical translation[244,245]. Moreover, AuNPs are chemically inert and non-toxic,

but their long-term effects on health are still uncertain, if a portion of the dose is retained in the body[246]. Recently, atomic AuNCs, which are ultrasmall clusters of 10–100 gold atoms (having a total diameter of <2 nm), have emerged as promising agents in cancer diagnosis and treatment. Owing to their small size, these AuNCs result in fast renal clearance with minimum retention in the MPS organs, such as liver and spleen[247]. As a result, renally clearable and biodegradable NP formulations are preferred for in vivo imaging applications to avoid any long-term toxicity concern. Although non-biodegradable NPs are being evaluated for their safety in vivo, they can still offer valuable information in both in vitro and ex vivo imaging studies. Nonetheless, the physicochemical characteristics of non-biodegradable NPs, such as composition and surface modifications, should be further investigated to understand the issue of toxicity effects and concerns related to their excretion profiles before they can be implemented for use in patient care. Current efforts should therefore be focused on developing NP structures that subsequently break down into nontoxic materials and harmless by-products for efficient elimination.

### Delivery

One of the biggest hurdles for clinical translation of any nano-based contrast agent is their effective delivery in a quantity that enables sensitive detection and localization[248]. Large amounts of NP agent are often required at the target site, especially when using less-sensitive imaging modalities, such as CT[249]. In particular, the EPR effect is a powerful delivery mechanism that allows NPs to passively accumulate in diseased tissues with sustained angiogenesis and a permeable vasculature (such as tumours, inflammation and atherosclerosis), although the magnitude of the EPR effect is variable depending on the individual[250]. Retention of these NPs at diseased sites has also been demonstrated as a result of their uptake by local pathologically associated macrophages[251]. It is essential that the NPs have long enough blood circulation times and stealthy coatings to effectively reach their target and evade uptake by other organs. Enhanced imaging specificity can be achieved by conjugating the NP surface with targeting moieties that have a high degree of molecular specificity. There are also other factors to take into consideration when optimizing for targeted NP delivery. For example, antibodies are highly specific towards their targets but can be expensive, and their attachment may increase the overall NP size by as much as 10 nm, thereby changing the pharmacological characteristics of the NP. Addition of antibodies and other biological linkages to an NP can result in further regulatory testing and increased developmental cost. Some linkages, such as biotin-streptavidin, may generate immunologic responses in patients. In such cases, ligands can be covalently attached to NPs using various methods, such as novel protein Z-mediated expressed protein ligation (EPL)-click reaction, that do not elicit an immune response in humans, but may still require additional regulatory testing[252].

### Commercial considerations

Most of the current NPs that are FDA-approved or in clinical trials involve therapeutics, whereas those for imaging agents are fewer[253,254]. This disparity may, in part, be due to the higher market potential for developing new therapies as opposed to new imaging agents. Unfortunately, the earning potential of diagnostic imaging contrast agents is much lower than that of therapeutic agents. The recently approved nano-based COVID vaccines

achieved sales over US$50 billion. The market clearly favours the therapeutic route[254]. It is a challenge to justify the costs to develop nano-based imaging agents when the return on the investment is low. Fortunately, there are several new and exciting opportunities for imaging to offer important insights to enable better therapeutic drug discovery and help guide therapeutic decisions. This opens up an entirely new market for the development of nano-based imaging contrast agents to offer rich molecular information about the disease of an individual patient, enabling a more effective treatment response and justifying the cost for clinical translation. Additionally, with a new generation of NP therapeutics likely to be forthcoming, spurred by the resounding success of the NP COVID vaccines, the clinical translation of new NP imaging contrast agents may be driven in part by the need for companion diagnostics (companion diagnostics are commonly required for targeted radiotherapeutics to determine whether the disease of the patient has the target and therefore whether the radiotherapeutic is likely to be effective).

## Outlook

Many preclinical studies have supported the use of nanomaterials as imaging agents given their tunable physicochemical properties and desired contrast enhancement. From the mid-1990s to mid-2000s, several IONP MRI contrast agents designed to diagnose and characterize focal liver lesions or liver metastasis were successfully translated into the clinic[255]. These NPs have been shown to outperform their small-molecule counterparts, such as $^{18}$F-FDG and gadolinium chelates, especially in hepatic cancer imaging; however, some formulations were withdrawn owing to low sales. Several gold nanomaterials, such as AuroShells, have also been investigated in clinical trials as cancer therapeutics[256]. These advances are considered a recent major milestone for the field, given that only a handful of NP formulations has been approved as diagnostics to date (Table 2). However, translational activity has since been low, partly owing to poor economic outlook for diagnostic agents and current market emphasis on nano-therapeutics. Another hindrance for clinical translation is that there is a lower tolerance for side effects for contrast agents than for therapeutics, which raises the bar for safety. Although contrast agents have lower standards for efficacy than therapeutics, simply binding a target, as opposed to increasing survival compared with current therapies, may render approval more likely.

With the recent surge in targeted immunotherapies, clinicians are eager for newly developed imaging and monitoring tools, including novel nanomaterial-based contrast agents and relevant detection techniques, to help predict patient response and personalize disease therapy on an individual basis. Non-invasive imaging strategies have the added benefit of offering longitudinal information to better determine the effectiveness of a given treatment over time. The ability of NPs to actively target tumour areas can help differentiate inflammation from tumour progression, thus providing a more reliable way to evaluate for treatment response. Furthermore, surgery is usually the first line of treatment for most patients with cancer diagnosed at stages I to III. Incomplete tumour resection often results in negative patient outcomes and decreased survival, as well as increased health-care costs owing to additional surgical interventions. Nano-based contrast agents have been shown to improve tumour margin delineation and assist in surgical resection through intraoperative, real-time image guidance with greater sensitivity and specificity. Notably, a recent phase

II clinical study has shown that ONM-100 (or pegsitacianine), a pH-sensitive, micellar fluorescence agent, could enhance the ability of a surgeon to detect residual malignancies following cytoreductive surgery of peritoneal metastases[85]. With these encouraging results, more research interest and funding support for this agent type in the coming years may be expected. Overall, intraoperative image guidance may considerably decrease the frequency of repeat surgeries and markedly reduce patient expenses, while justifying further development of these nano-based contrast agents with the possibility to overcome their market challenges.

In summary, nano-based imaging contrast agents have great potential to vastly improve disease detection and patient outcomes if further developed[257]. The field would benefit from greater interactions and collaboration among material scientists, academic researchers, radiologists, industries and regulatory agencies to guide the advancement of nano-based contrast agents, meet clinical demands and satisfy regulatory requirements. Nano-based imaging strategies can offer so much more than disease diagnosis. New studies have demonstrated their ability to present crucial insights to direct drug development and provide predictive information to guide therapeutic decisions. With this in mind, it is imperative to continue to promote the development of new nano-based contrast agents that can offer physicians invaluable structural and functional information about the disease progression within an individual.

## Acknowledgements

## Glossary

**Brust method**

A commonly used method to synthesize gold nanoparticles in non-aqueous solutions

**Contrast agents**

Substances administered in medical imaging procedures to facilitate disease diagnosis via altering image contrast

**Enhanced permeation and retention (EPR) effect**

The phenomenon of elevated retention of nanomaterials in certain diseased tissues (for example, tumours and sites of inflammation) owing to leaky vessels and poor lymphatic drainage

**Hot-spot imaging**

Imaging of certain tracers, such as fluorinated nanoparticles with $^{19}$F-magnetic resonance imaging, allows for specific detection in vivo without endogenous background signal

**Nano-based contrast agents**

Contrast agents that are within the nano-size range, typically 1–400 nm

**Phantom**

A device composed of tissue-equivalent materials that is used to evaluate imaging performance of contrast agents

**Quantum confinement effect**

When a critical threshold size (2–10 nm) is reached, nanomaterials present tunable fluorescence properties reflecting small differences in particle size

**$T_1$ agents**

Contrast agents for magnetic resonance imaging that are used to shorten $T_1$ relaxation. They typically involve gadolinium or manganese

**$T_2$-shortening agents**

Contrast agents for magnetic resonance imaging that are used to shorten $T_2$ relaxation. They are most frequently iron oxide nanoparticles

## References

1. Kim J et al. Use of nanoparticle contrast agents for cell tracking with computed tomography. Bioconjug. Chem 28, 1581–1597 (2017). [PubMed: 28485976]

2. Dong YC, Bouche M, Uman S, Burdick JA & Cormode DP Detecting and monitoring hydrogels with medical imaging. ACS Biomater. Sci. Eng 7, 4027–4047 (2021). [PubMed: 33979137]

3. Cormode DP, Skajaa T, Fayad ZA & Mulder WJ Nanotechnology in medical imaging: probe design and applications. Arterioscler. Thromb. Vasc. Biol 29, 992–1000 (2009). [PubMed: 19057023]

4. Choi HS et al. Renal clearance of quantum dots. Nat. Biotechnol 25, 1165–1170 (2007). [PubMed: 17891134] To our knowledge, this is the first paper to systemically study the nanoparticle size and ligand coatings required for rapid and efficient renal excretion.

5. Nieves LM et al. Renally excretable silver telluride nanoparticles as contrast agents for X-ray imaging. ACS Appl. Mater. Interfaces 14, 34354–34364 (2022). [PubMed: 35867906]

6. Zhou C, Long M, Qin Y, Sun X & Zheng J Luminescent gold nanoparticles with efficient renal clearance. Angew. Chem. Int. Ed 50, 3168–3172 (2011).

7. Cole LE, McGinnity TL, Irimata LE, Vargo-Gogola T & Roeder RK Effects of bisphosphonate ligands and PEGylation on targeted delivery of gold nanoparticles for contrast-enhanced radiographic detection of breast microcalcifications. Acta Biomater 82, 122–132 (2018). [PubMed: 30316022]

8. Sykes EA, Chen J, Zheng G & Chan WC Investigating the impact of nanoparticle size on active and passive tumor targeting efficiency. ACS Nano 8, 5696–5706 (2014). [PubMed: 24821383]

9. Li B & Lane LA Probing the biological obstacles of nanomedicine with gold nanoparticles. Wiley Interdiscip. Rev. Nanomed. Nanobiotechnol 11, e1542 (2019). [PubMed: 30084539]

10. Nakamura Y, Mochida A, Choyke PL & Kobayashi H Nanodrug delivery: is the enhanced permeability and retention effect sufficient for curing cancer? Bioconjug. Chem 27, 2225–2238 (2016). [PubMed: 27547843]

11. Nieves LM, Mossburg K, Hsu JC, Maidment ADA & Cormode DP Silver chalcogenide nanoparticles: a review of their biomedical applications. Nanoscale 13, 19306–19323 (2021). [PubMed: 34783806]

12. Bouche M et al. Recent advances in molecular imaging with gold nanoparticles. Bioconjug. Chem 31, 303–314 (2020). [PubMed: 31682405]

13. Cormode DP, Naha PC & Fayad ZA Nanoparticle contrast agents for computed tomography: a focus on micelles. Contrast Media Mol. Imaging 9, 37–52 (2014). [PubMed: 24470293]

14. Mulder WJ et al. Nanoparticulate assemblies of amphiphiles and diagnostically active materials for multimodality imaging. Acc. Chem. Res 42, 904–914 (2009). [PubMed: 19435319]

15. Baig RBN & Varma RS Alternative energy input: mechanochemical, microwave and ultrasound-assisted organic synthesis. Chem. Soc. Rev 41, 1559–1584 (2012). [PubMed: 22076552]

16. Smith BR & Gambhir SS Nanomaterials for in vivo imaging. Chem. Rev 117, 901–986 (2017). [PubMed: 28045253]

17. James ML & Gambhir SS A molecular imaging primer: modalities, imaging agents, and applications. Physiol. Rev 92, 897–965 (2012). [PubMed: 22535898]

18. Padmanabhan P, Kumar A, Kumar S, Chaudhary RK & Gulyás B Nanoparticles in practice for molecular-imaging applications: an overview. Acta Biomater 41, 1–16 (2016). [PubMed: 27265153]

19. Jendrasiak GL, Frey GD & Heim RC Jr Liposomes as carriers of iodolipid radiocontrast agents for CT scanning of the liver. Invest. Radiol 20, 995–1002 (1985). [PubMed: 3000977] This work introduces iodinated liposomes as one of the first nanoparticle-based CT contrast agents.

20. Gazelle GS et al. Hepatic imaging with iodinated nanoparticles: a comparison with iohexol in rabbits. Acad. Radiol 2, 700–704 (1995). [PubMed: 9419627]

21. Seltzer SE, Gregoriadis G & Dick R Evaluation of the dehydration–rehydration method for production of contrast-carrying liposomes. Invest. Radiol 23, 131–138 (1988). [PubMed: 3343110]

22. Hsu JC et al. Nanoparticle contrast agents for X-ray imaging applications. Wiley Interdiscip. Rev. Nanomed. Nanobiotechnol 12, e1642 (2020). [PubMed: 32441050]

23. Naha PC et al. Dextran-coated cerium oxide nanoparticles: a computed tomography contrast agent for imaging the gastrointestinal tract and inflammatory bowel disease. ACS Nano 14, 10187–10197 (2020). [PubMed: 32692538]

24. Karunamuni R, Tsourkas A & Maidment AD Exploring silver as a contrast agent for contrast-enhanced dual-energy X-ray breast imaging. Br. J. Radiol 87, 20140081 (2014). [PubMed: 24998157]

25. Karunamuni R & Maidment AD Search for novel contrast materials in dual-energy X-ray breast imaging using theoretical modeling of contrast-to-noise ratio. Phys. Med. Biol 59, 4311–4324 (2014). [PubMed: 25029534]

26. Lee SH, Kim BH, Na HB & Hyeon T Paramagnetic inorganic nanoparticles as T1 MRI contrast agents. Wiley Interdiscip. Rev. Nanomed. Nanobiotechnol 6, 196–209 (2014). [PubMed: 24123961]

27. Mulder WJ, Strijkers GJ, van Tilborg GA, Griffioen AW & Nicolay K Lipid-based nanoparticles for contrast-enhanced MRI and molecular imaging. NMR Biomed 19, 142–164 (2006). [PubMed: 16450332]

28. Dadfar SM et al. Iron oxide nanoparticles: diagnostic, therapeutic and theranostic applications. Adv. Drug Deliv. Rev 138, 302–325 (2019). [PubMed: 30639256]

29. Hu Y, Mignani S, Majoral JP, Shen M & Shi X Construction of iron oxide nanoparticle-based hybrid platforms for tumor imaging and therapy. Chem. Soc. Rev 47, 1874–1900 (2018). [PubMed: 29376542]

30. Ali MM et al. A nano-sized PARACEST-fluorescence imaging contrast agent facilitates and validates in vivo CEST MRI detection of glioma. Nanomedicine 7, 1827–1837 (2012). [PubMed: 22891866] This study presents a dual-modality PARACEST and fluorescent contrast agent based on dendrimers conjugated with europium–DOTA–tetraglycinate and a fluorophore.

31. Chan KW, Bulte JW & McMahon MT Diamagnetic chemical exchange saturation transfer (diaCEST) liposomes: physicochemical properties and imaging applications. Wiley Interdiscip. Rev. Nanomed. Nanobiotechnol 6, 111–124 (2014). [PubMed: 24339357]

32. Wang C, Adams SR & Ahrens ET Emergent fluorous molecules and their uses in molecular imaging. Acc. Chem. Res 54, 3060–3070 (2021). [PubMed: 34259521]

33. Ashur I, Allouche-Arnon H & Bar-Shir A Calcium fluoride nanocrystals: tracers for in vivo (19) F magnetic resonance imaging. Angew. Chem. Int. Ed 57, 7478–7482 (2018).

34. Duong HTK et al. A guide to the design of magnetic particle imaging tracers for biomedical applications. Nanoscale 14, 13890–13914 (2022). [PubMed: 36004758]

35. Irfan M & Dogan N Comprehensive evaluation of magnetic particle imaging (MPI) scanners for biomedical applications. IEEE Access 10, 86718–86732 (2022).

36. Chakravarty R, Hong H & Cai W Positron emission tomography image-guided drug delivery: current status and future perspectives. Mol. Pharm 11, 3777–3797 (2014). [PubMed: 24865108]

37. Goel S, England CG, Chen F & Cai W Positron emission tomography and nanotechnology: a dynamic duo for cancer theranostics. Adv. Drug Deliv. Rev 113, 157–176 (2017). [PubMed: 27521055]

38. Sun X, Cai W & Chen X Positron emission tomography imaging using radiolabeled inorganic nanomaterials. Acc. Chem. Res 48, 286–294 (2015). [PubMed: 25635467]

39. Ametamey SM, Honer M & Schubiger PA Molecular imaging with PET. Chem. Rev 108, 1501–1516 (2008). [PubMed: 18426240]

40. Medintz IL, Uyeda HT, Goldman ER & Mattoussi H Quantum dot bioconjugates for imaging, labelling and sensing. Nat. Mater 4, 435–446 (2005). [PubMed: 15928695]

41. Jiang P, Zhu CN, Zhang ZL, Tian ZQ & Pang DW Water-soluble Ag(2)S quantum dots for near-infrared fluorescence imaging in vivo. Biomaterials 33, 5130–5135 (2012). [PubMed: 22484042]

42. Li W & Chen X Gold nanoparticles for photoacoustic imaging. Nanomedicine 10, 299–320 (2015). [PubMed: 25600972]

43. Hajfathalian M et al. Wulff in a cage gold nanoparticles as contrast agents for computed tomography and photoacoustic imaging. Nanoscale 10, 18749–18757 (2018). [PubMed: 30276391]

44. Xie C, Zhen X, Lei Q, Ni R & Pu K Self-assembly of semiconducting polymer amphiphiles for in vivo photoacoustic imaging. Adv. Funct. Mater 27, 1605397 (2017).This work describes the first generation of amphiphilic optically active semiconducting polymer nanoparticles for PA and fluorescence imaging.

45. Klibanov AL Ultrasound contrast: gas microbubbles in the vasculature. Invest. Radiol 56, 50–61 (2021). [PubMed: 33181574]

46. Exner AA & Kolios MC Bursting microbubbles: how nanobubble contrast agents can enable the future of medical ultrasound molecular imaging and image-guided therapy. Curr. Opin. Colloid. Interface. Sci 10.1016/j.cocis.2021.101463 (2021).This review summarizes the recent developments of acoustically active nanobubbles as ultrasound contrast agents and as therapeutic vehicles.

47. Duan H, Wang D & Li Y Green chemistry for nanoparticle synthesis. Chem. Soc. Rev 44, 5778–5792 (2015). [PubMed: 25615873]

48. Tao H et al. Nanoparticle synthesis assisted by machine learning. Nat. Rev. Mater 6, 701–716 (2021).

49. Gao J, Wu C, Deng D, Wu P & Cai C Direct synthesis of water-soluble aptamer-Ag2 S quantum dots at ambient temperature for specific imaging and photothermal therapy of cancer. Adv. Healthc. Mater 5, 2437–2449 (2016). [PubMed: 27391840]

50. Hsu JC et al. Effect of nanoparticle synthetic conditions on ligand coating integrity and subsequent nano–biointeractions. ACS Appl. Mater. Interfaces 13, 58401–58410 (2021). [PubMed: 34846845]

51. Kim D, Kim J, Park YI, Lee N & Hyeon T Recent development of inorganic nanoparticles for biomedical imaging. ACS Cent. Sci 4, 324–336 (2018). [PubMed: 29632878]

52. Dong YC et al. Effect of gold nanoparticle size on their properties as contrast agents for computed tomography. Sci. Rep 9, 14912 (2019). [PubMed: 31624285]

53. Luo D, Wang X, Burda C & Basilion JP Recent development of gold nanoparticles as contrast agents for cancer diagnosis. Cancers 10.3390/cancers13081825 (2021).

54. Jokerst JV, Cole AJ, Van de Sompel D & Gambhir SS Gold nanorods for ovarian cancer detection with photoacoustic imaging and resection guidance via Raman imaging in living mice. ACS Nano 6, 10366–10377 (2012). [PubMed: 23101432]

55. Xu P et al. A DM1-doped porous gold nanoshell system for NIR accelerated redox-responsive release and triple modal imaging guided photothermal synergistic chemotherapy. J. Nanobiotechnol 19, 77 (2021).

56. Kim BH et al. Large-scale synthesis of uniform and extremely small-sized iron oxide nanoparticles for high-resolution T1 magnetic resonance imaging contrast agents. J. Am. Chem. Soc 133, 12624–12631 (2011). [PubMed: 21744804]

57. Peng Y-K, Tsang SCE & Chou P-T Chemical design of nanoprobes for T1-weighted magnetic resonance imaging. Mater. Today 19, 336–348 (2016).

58. Kim J et al. High-quantum yield alloy-typed core/shell CdSeZnS/ZnS quantum dots for bio-applications. J. Nanobiotechnol 20, 22 (2022).

59. Shreyash N et al. Green synthesis of nanoparticles and their biomedical applications: a review. ACS Appl. Nano Mater 4, 11428–11457 (2021).

60. Xiao L et al. Enhanced in vitro and in vivo cellular imaging with green tea coated water-soluble iron oxide nanocrystals. ACS Appl. Mater. Interfaces 7, 6530–6540 (2015). [PubMed: 25729881]

61. Wu L et al. A green synthesis of carbon nanoparticle from honey for real-time photoacoustic imaging. Nano Res 6, 312–325 (2013). [PubMed: 23824757]

62. Tassa C, Shaw SY & Weissleder R Dextran-coated iron oxide nanoparticles: a versatile platform for targeted molecular imaging, molecular diagnostics, and therapy. Acc. Chem. Res 44, 842–852 (2011). [PubMed: 21661727]

63. Naha PC et al. Dextran coated bismuth–iron oxide nanohybrid contrast agents for computed tomography and magnetic resonance imaging. J. Mater. Chem. B 2, 8239–8248 (2014). [PubMed: 25485115]

64. Kim J et al. Ultrasmall antioxidant cerium oxide nanoparticles for regulation of acute inflammation. ACS Appl. Mater. Interfaces 13, 60852–60864 (2021). [PubMed: 34914872]

65. Cormode DP, Jarzyna PA, Mulder WJ & Fayad ZA Modified natural nanoparticles as contrast agents for medical imaging. Adv. Drug Deliv. Rev 62, 329–338 (2010). [PubMed: 19900496]

66. Lobatto ME et al. Multimodal positron emission tomography imaging to quantify uptake of 89Zr-labeled liposomes in the atherosclerotic vessel wall. Bioconjug. Chem 31, 360–368 (2020). [PubMed: 31095372]

67. Lin W et al. Doxorubicin-loaded unimolecular micelle-stabilized gold nanoparticles as a theranostic nanoplatform for tumor-targeted chemotherapy and computed tomography Imaging. Biomacromolecules 18, 3869–3880 (2017). [PubMed: 29032674]

68. Guo M et al. Dual imaging-guided photothermal/photodynamic therapy using micelles. Biomaterials 35, 4656–4666 (2014). [PubMed: 24613048]

69. Cormode DP et al. Nanocrystal core high-density lipoproteins: a multimodality contrast agent platform. Nano Lett 8, 3715–3723 (2008). [PubMed: 18939808] This work uses HDL to create various nanoparticle–inorganic material composites for multimodality imaging of atherosclerosis.

70. Rakhshan S, Alberti D, Stefania R, Bitonto V & Geninatti Crich S LDL mediated delivery of paclitaxel and MRI imaging probes for personalized medicine applications. J. Nanobiotechnol 19, 208 (2021).

71. Perez-Medina C et al. PET imaging of tumor-associated macrophages with 89Zr-labeled high-density lipoprotein nanoparticles. J. Nucl. Med 56, 1272–1277 (2015). [PubMed: 26112022]

72. Sanchez-Gaytan BL et al. HDL-mimetic PLGA nanoparticle to target atherosclerosis plaque macrophages. Bioconjug. Chem 26, 443–451 (2015). [PubMed: 25650634]

73. Pérez-Medina C et al. In vivo PET imaging of HDL in multiple atherosclerosis models. JACC Cardiovasc. Imaging 9, 950–961 (2016). [PubMed: 27236528]

74. Yuan Y et al. Furin-mediated intracellular self-assembly of olsalazine nanoparticles for enhanced magnetic resonance imaging and tumour therapy. Nat. Mater 18, 1376–1383 (2019). [PubMed: 31636420] This study describes the self-assembly of a peptide–drug conjugate into large intracellular NPs via the activity of furin, a tumour-associated enzyme, for enhanced cancer theranostics.

75. Yuan Y et al. Furin-mediated self-assembly of olsalazine nanoparticles for targeted Raman imaging of tumors. Angew. Chem. Int. Ed 60, 3923–3927 (2021).

76. Srikar R, Upendran A & Kannan R Polymeric nanoparticles for molecular imaging. Wiley Interdiscip. Rev. Nanomed. Nanobiotechnol 6, 245–267 (2014). [PubMed: 24616442]

77. Pu K et al. Semiconducting polymer nanoparticles as photoacoustic molecular imaging probes in living mice. Nat. Nanotechnol 9, 233–239 (2014). [PubMed: 24463363]

78. Pu K et al. Diketopyrrolopyrrole-based semiconducting polymer nanoparticles for in vivo photoacoustic imaging. Adv. Mater 27, 5184–5190 (2015). [PubMed: 26247171]

79. Cheheltani R et al. Tunable, biodegradable gold nanoparticles as contrast agents for computed tomography and photoacoustic imaging. Biomaterials 102, 87–97 (2016). [PubMed: 27322961]

80. Peng C et al. PEGylated dendrimer-entrapped gold nanoparticles for in vivo blood pool and tumor imaging by computed tomography. Biomaterials 33, 1107–1119 (2012). [PubMed: 22061490]

81. Zhao J et al. CREKA peptide-conjugated dendrimer nanoparticles for glioblastoma multiforme delivery. J. Colloid Interface Sci 450, 396–403 (2015). [PubMed: 25863222]

82. Chen M et al. Multifunctional dendrimer-entrapped gold nanoparticles for labeling and tracking T cells via dual-modal computed tomography and fluorescence imaging. Biomacromolecules 21, 1587–1595 (2020). [PubMed: 32154709]

83. Cai QY et al. Colloidal gold nanoparticles as a blood-pool contrast agent for X-ray computed tomography in mice. Invest. Radiol 42, 797–806 (2007). [PubMed: 18007151]

84. Xie J, Gao J, Michalski M & Chen X in Nanoplatform-based Molecular Imaging (ed. Chen X) 47–73 (Wiley, 2011).

85. Voskuil FJ et al. Exploiting metabolic acidosis in solid cancers using a tumor-agnostic pH-activatable nanoprobe for fluorescence-guided surgery. Nat. Commun 11, 3257 (2020). [PubMed: 32591522]

86. Yu MK, Park J & Jon S Targeting strategies for multifunctional nanoparticles in cancer imaging and therapy. Theranostics 2, 3–44 (2012). [PubMed: 22272217] This review provides a comprehensive summary of targeting strategies, targeting moieties and conjugation methods used for functionalizing NP agents.

87. Mao W, Kim HS, Son YJ, Kim SR & Yoo HS Doxorubicin encapsulated clicked gold nanoparticle clusters exhibiting tumor-specific disassembly for enhanced tumor localization and computerized tomographic imaging. J. Control. Release 269, 52–62 (2018). [PubMed: 29113793]

88. Cai W et al. Peptide-labeled near-infrared quantum dots for imaging tumor vasculature in living subjects. Nano Lett 6, 669–676 (2006). [PubMed: 16608262]

89. Allijn IE et al. Gold nanocrystal labeling allows low-density lipoprotein imaging from the subcellular to macroscopic level. ACS Nano 7, 9761–9770 (2013). [PubMed: 24127782]

90. Cho EJ et al. Nanoparticle characterization: state of the art, challenges, and emerging technologies. Mol. Pharm 10, 2093–2110 (2013). [PubMed: 23461379] This review offers a critical review of current and emerging in vitro and in vivo techniques used for characterizing NP agents.

91. Lim J, Yeap SP, Che HX & Low SC Characterization of magnetic nanoparticle by dynamic light scattering. Nanoscale Res. Lett 8, 381 (2013). [PubMed: 24011350]

92. Eaton P et al. A direct comparison of experimental methods to measure dimensions of synthetic nanoparticles. Ultramicroscopy 182, 179–190 (2017). [PubMed: 28692935]

93. Bhattacharjee S DLS and zeta potential — what they are and what they are not? J. Control. Relase 235, 337–351 (2016).

94. Filipe V, Hawe A & Jiskoot W Critical evaluation of nanoparticle tracking analysis (NTA) by NanoSight for the measurement of nanoparticles and protein aggregates. Pharm. Res 27, 796–810 (2010). [PubMed: 20204471]

95. Jazani S et al. An alternative framework for fluorescence correlation spectroscopy. Nat. Commun 10, 3662 (2019). [PubMed: 31413259]

96. Kim A, Ng WB, Bernt W & Cho NJ Validation of size estimation of nanoparticle tracking analysis on polydisperse macromolecule assembly. Sci. Rep 9, 2639 (2019). [PubMed: 30804441]

97. Glasscott MW, Pendergast AD, Choudhury MH & Dick JE Advanced characterization techniques for evaluating porosity, nanopore tortuosity, and electrical connectivity at the single-nanoparticle level. ACS Appl. Nano Mater 2, 819–830 (2019).

98. Mourdikoudis S, Pallares RM & Thanh NTK Characterization techniques for nanoparticles: comparison and complementarity upon studying nanoparticle properties. Nanoscale 10, 12871–12934 (2018). [PubMed: 29926865]

99. Barenholz Y & Amselem SJLT Quality control assays in the development and clinical use of liposome-based formulations. Pharmaceutics 1, 527–616 (1993).

100. Moore TL et al. Nanoparticle colloidal stability in cell culture media and impact on cellular interactions. Chem. Soc. Rev 44, 6287–6305 (2015). [PubMed: 26056687]

101. Baimanov D, Cai R & Chen C Understanding the chemical nature of nanoparticle–protein interactions. Bioconjug. Chem 30, 1923–1937 (2019). [PubMed: 31259537]

102. Bouche M et al. Novel treatment for glioblastoma delivered by a radiation responsive and radiopaque hydrogel. ACS Biomater. Sci. Eng 7, 3209–3220 (2021). [PubMed: 34160196]

103. Zhang G, Naha PC, Gautam P, Cormode DP & Chan JMW Water-dispersible bismuth-organic materials with computed tomography contrast properties. ACS Appl. Bio Mater 1, 1918–1926 (2018).

104. Si-Mohamed S et al. Evaluation of spectral photon counting computed tomography K-edge imaging for determination of gold nanoparticle biodistribution in vivo. Nanoscale 9, 18246–18257 (2017). [PubMed: 28726968]

105. Kim J et al. Radioprotective garment-inspired biodegradable polymetal nanoparticles for enhanced CT contrast production. Chem. Mater 32, 381–391 (2020). [PubMed: 33005071]

106. Zhang Z & Seeram E The use of artificial intelligence in computed tomography image reconstruction — a literature review. J. Med. Imaging Radiat. Sci 51, 671–677 (2020). [PubMed: 32981888]

107. Lauritzen AD et al. An artificial intelligence-based mammography screening protocol for breast cancer: outcome and radiologist workload. Radiology 304, 41–49 (2022). [PubMed: 35438561]

108. Galper MW et al. Effect of computed tomography scanning parameters on gold nanoparticle and iodine contrast. Invest. Radiol 47, 475–481 (2012). [PubMed: 22766909]

109. Hsu JC et al. Renally excretable and size-tunable silver sulfide nanoparticles for dual-energy mammography or computed tomography. Chem. Mater 31, 7845–7854 (2019). [PubMed: 33005070]

110. Kim J et al. Assessment of candidate elements for development of spectral photon-counting CT specific contrast agents. Sci. Rep 8, 12119 (2018). [PubMed: 30108247]

111. Christoffersson JO, Olsson LE & Sjoberg S Nickel-doped agarose gel phantoms in MR imaging. Acta Radiol 32, 426–431 (1991). [PubMed: 1911001]

112. Jeon M, Halbert MV, Stephen ZR & Zhang M Iron oxide nanoparticles as T1 contrast agents for magnetic resonance imaging: fundamentals, challenges, applications, and prospectives. Adv. Mater 33, 1906539 (2021).

113. Jahromi AH et al. Fluorous-soluble metal chelate for sensitive fluorine-19 magnetic resonance imaging nanoemulsion probes. ACS Nano 13, 143–151 (2019). [PubMed: 30525446] This work presents a nanoemulsion probe based on a fluorophilic chelating agent for hot-spot detection of inflammation-associated macrophages via $^{19}$F MRI.

114. Kenny GD et al. A bisphosphonate for (19)F-magnetic resonance imaging. J. Fluor. Chem 184, 58–64 (2016). [PubMed: 27110036]

115. Lesniak WG et al. Salicylic acid conjugated dendrimers are a tunable, high performance CEST MRI nanoplatform. Nano Lett 16, 2248–2253 (2016). [PubMed: 26910126]

116. Chen F et al. In vivo integrity and biological fate of chelator-free zirconium-89-labeled mesoporous silica nanoparticles. ACS Nano 9, 7950–7959 (2015). [PubMed: 26213260]

117. Ni D et al. Ceria nanoparticles meet hepatic ischemia–reperfusion injury: the perfect imperfection. Adv. Mater 31, e1902956 (2019). [PubMed: 31418951]

118. Xu C et al. Bacteria-like mesoporous silica-coated gold nanorods for positron emission tomography and photoacoustic imaging-guided chemo-photothermal combined therapy. Biomaterials 165, 56–65 (2018). [PubMed: 29501970] This study demonstrates the utility of drug-loaded mesoporous silica-coated gold nanorods for PET/PAI-guided combination therapy and triggered drug release for enhanced cancer theranostics.

119. Higbee-Dempsey E et al. Indocyanine green-coated gold nanoclusters for photoacoustic imaging and photothermal therapy. Adv. Ther 10.1002/adtp.201900088 (2019).

120. Bohndiek SE, Bodapati S, Van De Sompel D, Kothapalli SR & Gambhir SS Development and application of stable phantoms for the evaluation of photoacoustic imaging instruments. PLoS ONE 8, e75533 (2013). [PubMed: 24086557]

121. Teraphongphom N et al. Nanoparticle loaded polymeric microbubbles as contrast agents for multimodal imaging. Langmuir 31, 11858–11867 (2015). [PubMed: 26446176]

122. Henriksen-Lacey M, Carregal-Romero S & Liz-Marzán LM Current challenges toward in vitro cellular validation of inorganic nanoparticles. Bioconjug. Chem 28, 212–221 (2017). [PubMed: 27709892]

123. De Lorenzi F et al. Profiling target engagement and cellular uptake of cRGD-decorated clinical-stage core-crosslinked polymeric micelles. Drug Deliv. Transl. Res 10.1007/s13346-022-01204-8 (2022).

124. Ruenraroengsak P & Tetley TD Differential bioreactivity of neutral, cationic and anionic polystyrene nanoparticles with cells from the human alveolar compartment: robust response of alveolar type 1 epithelial cells. Part. Fibre Toxicol 12, 19 (2015). [PubMed: 26133975]

125. Rosenkrans ZT et al. Selenium-doped carbon quantum dots act as broad-spectrum antioxidants for acute kidney injury management. Adv. Sci 7, 2000420 (2020).

126. Shilo M, Reuveni T, Motiei M & Popovtzer R Nanoparticles as computed tomography contrast agents: current status and future perspectives. Nanomedicine 7, 257–269 (2012). [PubMed: 22339135]

127. Cormode DP et al. Multicolor spectral photon-counting computed tomography: in vivo dual contrast imaging with a high count rate scanner. Sci. Rep 7, 4784 (2017). [PubMed: 28684756]

128. Hallouard F et al. Radiopaque iodinated nano-emulsions for preclinical X-ray imaging. RSC Adv 1, 792–801 (2011).

129. Ghaghada KB, Sato AF, Starosolski ZA, Berg J & Vail DM Computed tomography imaging of solid tumors using a liposomal-iodine contrast agent in companion dogs with naturally occurring cancer. PLoS ONE 11, e0152718 (2016). [PubMed: 27031614]

130. Yin Q et al. Poly(iohexol) nanoparticles as contrast agents for in vivo X-ray computed tomography imaging. J. Am. Chem. Soc 135, 13620–13623 (2013). [PubMed: 23987119]

131. Hsu JC et al. An all-in-one nanoparticle (AION) contrast agent for breast cancer screening with DEM-CT-MRI-NIRF imaging. Nanoscale 10, 17236–17248 (2018). [PubMed: 30191237] This is the first study to develop silver telluride NPs as a novel contrast agent for breast imaging with DEM.

132. Naha PC et al. Gold silver alloy nanoparticles (GSAN): an imaging probe for breast cancer screening with dual-energy mammography or computed tomography. Nanoscale 8, 13740–13754 (2016). [PubMed: 27412458]

133. Nieves LM, Hsu JC, Lau KC, Maidment ADA & Cormode DP Silver telluride nanoparticles as biocompatible and enhanced contrast agents for X-ray imaging: an in vivo breast cancer screening study. Nanoscale 13, 163–174 (2021). [PubMed: 33325953]

134. Yin L, Zhang K, Sun Y & Liu Z Nanoparticle-assisted diagnosis and treatment for abdominal aortic aneurysm. Front. Med 8, 665846 (2021).

135. Si-Mohamed SA et al. In vivo molecular k-edge imaging of atherosclerotic plaque using photon-counting CT. Radiology 300, 98–107 (2021). [PubMed: 33944628] This report illustrates the use of spectral photon-counting CT in combination with gold NPs to detect and quantify atherosclerotic macrophages.

136. Cormode DP et al. Atherosclerotic plaque composition: analysis with multicolor CT and targeted gold nanoparticles. Radiology 256, 774–782 (2010). [PubMed: 20668118]

137. Meir R & Popovtzer R Cell tracking using gold nanoparticles and computed tomography imaging. Wiley Interdiscip. Rev. Nanomed. Nanobiotechnol 10.1002/wnan.1480 (2018).

138. Astolfo A et al. In vivo visualization of gold-loaded cells in mice using X-ray computed tomography. Nanomedicine 9, 284–292 (2013). [PubMed: 22841913]

139. Betzer O et al. In-vitro optimization of nanoparticle-cell labeling protocols for in-vivo cell tracking applications. Sci. Rep 5, 15400 (2015). [PubMed: 26507853]

140. Meir R et al. Nanomedicine for cancer immunotherapy: tracking cancer-specific T-cells in vivo with gold nanoparticles and CT imaging. ACS Nano 9, 6363–6372 (2015). [PubMed: 26039633] This report evaluates the migration and distribution of gold NP-labelled T cells via CT imaging, which exemplifies the application of CT to cell tracking.

141. Kim T et al. In vivo micro-CT imaging of human mesenchymal stem cells labeled with gold-poly-l-lysine nanocomplexes. Adv. Funct. Mater 10.1002/adfm.201604213 (2017).

Author Manuscript

142. Chhour P et al. Effect of gold nanoparticle size and coating on labeling monocytes for CT tracking. Bioconjug. Chem 28, 260–269 (2017). [PubMed: 28095688]

143. Ashton JR et al. Dual-energy CT imaging of tumor liposome delivery after gold nanoparticle-augmented radiation therapy. Theranostics 8, 1782–1797 (2018). [PubMed: 29556356]

144. Yu N et al. Thiol-capped Bi nanoparticles as stable and all-in-one type theranostic nanoagents for tumor imaging and thermoradiotherapy. Biomaterials 161, 279–291 (2018). [PubMed: 29425848]

145. FitzGerald PF et al. A proposed computed tomography contrast agent using carboxybetaine zwitterionic tantalum oxide nanoparticles: imaging, biological, and physicochemical performance. Invest. Radiol 51, 786–796 (2016). [PubMed: 27115702] This work presents a tantalum oxide NP CT contrast agent with one of the highest renal clearance efficiencies reported to date.

146. Dong YC et al. Ytterbium nanoparticle contrast agents for conventional and spectral photon-counting CT and their applications for hydrogel imaging. ACS Appl. Mater. Interfaces 14, 39274–39284 (2022). [PubMed: 35975982]

147. Li Y et al. Spectral computed tomography with inorganic nanomaterials: state-of-the-art. Adv. Drug Deliv. Rev 189, 114524 (2022). [PubMed: 36058350]

148. Shin TH, Choi Y, Kim S & Cheon J Recent advances in magnetic nanoparticle-based multi-modal imaging. Chem. Soc. Rev 44, 4501–4516 (2015). [PubMed: 25652670]

149. Huang Y, Hsu JC, Koo H & Cormode DP Repurposing ferumoxytol: diagnostic and therapeutic applications of an FDA-approved nanoparticle. Theranostics 12, 796–816 (2022). [PubMed: 34976214]

150. Zhao Z et al. Recent advances in engineering iron oxide nanoparticles for effective magnetic resonance imaging. Bioact. Mater 12, 214–245 (2022). [PubMed: 35310380]

151. Chen W et al. Collagen-specific peptide conjugated HDL nanoparticles as MRI contrast agent to evaluate compositional changes in atherosclerotic plaque regression. JACC Cardiovasc. Imaging 6, 373–384 (2013). [PubMed: 23433925]

152. Ni D et al. Integrating anatomic and functional dual-mode magnetic resonance imaging: design and applicability of a bifunctional contrast agent. ACS Nano 10, 3783–3790 (2016). [PubMed: 26910513]

153. Xiao J et al. Ultrahigh relaxivity and safe probes of manganese oxide nanoparticles for in vivo imaging. Sci. Rep 3, 3424 (2013). [PubMed: 24305731]

154. Zhen Z & Xie J Development of manganese-based nanoparticles as contrast probes for magnetic resonance imaging. Theranostics 2, 45–54 (2012). [PubMed: 22272218]

155. Kim T et al. Mesoporous silica-coated hollow manganese oxide nanoparticles as positive T1 contrast agents for labeling and MRI tracking of adipose-derived mesenchymal stem cells. J. Am. Chem. Soc 133, 2955–2961 (2011). [PubMed: 21314118]

156. Shin J et al. Hollow manganese oxide nanoparticles as multifunctional agents for magnetic resonance imaging and drug delivery. Angew. Chem. Int. Ed 48, 321–324 (2009).

157. Huang G et al. Tunable T1 and T2 contrast abilities of manganese-engineered iron oxide nanoparticles through size control. Nanoscale 6, 10404–10412 (2014). [PubMed: 25079966] This report examines the effect of nanoparticle size on the mode of detection as well as contrast generation in MRI.

158. Toth GB et al. Current and potential imaging applications of ferumoxytol for magnetic resonance imaging. Kidney Int 92, 47–66 (2017). [PubMed: 28434822] This review provides details on the properties and applications of ferumoxytol in contrast-enhanced MRI.

159. Cormode DP, Sanchez-Gaytan BL, Mieszawska AJ, Fayad ZA & Mulder WJ Inorganic nanocrystals as contrast agents in MRI: synthesis, coating and introduction of multifunctionality. NMR Biomed 26, 766–780 (2013). [PubMed: 23303729]

160. Daldrup-Link HE et al. MRI of tumor-associated macrophages with clinically applicable iron oxide nanoparticles. Clin. Cancer Res 17, 5695–5704 (2011). [PubMed: 21791632]

161. Daldrup-Link HE et al. Detection of stem cell transplant rejection with ferumoxytol MR imaging: correlation of MR imaging findings with those at intravital microscopy. Radiology 284, 495–507 (2017). [PubMed: 28128708]

162. Ahrens ET & Bulte JW Tracking immune cells in vivo using magnetic resonance imaging. Nat. Rev. Immunol 13, 755–763 (2013). [PubMed: 24013185]

163. Chen W, Cormode DP, Fayad ZA & Mulder WJM Nanoparticles as magnetic resonance imaging contrast agents for vascular and cardiac diseases. Wiley Interdiscip. Rev. Nanomed. Nanobiotechnol 3, 146–161 (2011). [PubMed: 20967875]

164. Ghosh D et al. M13-templated magnetic nanoparticles for targeted in vivo imaging of prostate cancer. Nat. Nanotechnol 7, 677–682 (2012). [PubMed: 22983492]

165. Gallo J et al. CXCR4-targeted and MMP-responsive iron oxide nanoparticles for enhanced magnetic resonance imaging. Angew. Chem. Int. Ed 53, 9550–9554 (2014).

166. Lee JH et al. High-contrast in vivo visualization of microvessels using novel FeCo/GC magnetic nanocrystals. Magn. Reson. Med 62, 1497–1509 (2009). [PubMed: 19859938]

167. Wang Q et al. Artificially engineered cubic iron oxide nanoparticle as a high-performance magnetic particle imaging tracer for stem cell tracking. ACS Nano 14, 2053–2062 (2020). [PubMed: 31999433]

168. Song G et al. Carbon-coated FeCo nanoparticles as sensitive magnetic-particle-imaging tracers with photothermal and magnetothermal properties. Nat. Biomed. Eng 4, 325–334 (2020). [PubMed: 32015409]

169. Cutler CS, Hennkens HM, Sisay N, Huclier-Markai S & Jurisson SS Radiometals for combined imaging and therapy. Chem. Rev 113, 858–883 (2013). [PubMed: 23198879]

170. Chen F et al. Ultrasmall targeted nanoparticles with engineered antibody fragments for imaging detection of HER2-overexpressing breast cancer. Nat. Commun 9, 4141 (2018). [PubMed: 30297810]

171. Yu B et al. Reassembly of (89) Zr-labeled cancer cell membranes into multicompartment membrane-derived liposomes for PET-trackable tumor-targeted theranostics. Adv. Mater 30, e1704934 (2018). [PubMed: 29430735]

172. Bhatnagar P et al. Imaging of genetically engineered T cells by PET using gold nanoparticles complexed to copper-64. Integr. Biol 5, 231–238 (2013).

173. Orbay H, Hong H, Zhang Y & Cai W Positron emission tomography imaging of atherosclerosis. Theranostics 3, 894–902 (2013). [PubMed: 24312158]

174. Majmudar MD et al. Polymeric nanoparticle PET/MR imaging allows macrophage detection in atherosclerotic plaques. Circ. Res 112, 755–761 (2013). [PubMed: 23300273]

175. Cheng L et al. Chelator-free labeling of metal oxide nanostructures with zirconium-89 for positron emission tomography imaging. ACS Nano 11, 12193–12201 (2017). [PubMed: 29178789] This work presents a general and simple method for chelator-free radiolabelling of various metal oxide nanostructures for PET imaging.

176. Chrastina A & Schnitzer JE Iodine-125 radiolabeling of silver nanoparticles for in vivo SPECT imaging. Int. J. Nanomed 5, 653–659 (2010).

177. Esposito E et al. Biodistribution of nanostructured lipid carriers: a tomographic study. Eur. J. Pharm. Biopharm 89, 145–156 (2015). [PubMed: 25497177]

178. Zhang Y et al. Positron emission tomography imaging of CD105 expression with a 64Cu-labeled monoclonal antibody: NOTA is superior to DOTA. PLoS ONE 6, e28005 (2011). [PubMed: 22174762]

179. Yang X et al. cRGD-functionalized, DOX-conjugated, and (6)(4)Cu-labeled superparamagnetic iron oxide nanoparticles for targeted anticancer drug delivery and PET/MR imaging. Biomaterials 32, 4151–4160 (2011). [PubMed: 21367450]

180. Chen F et al. In vivo tumor targeting and image-guided drug delivery with antibody-conjugated, radiolabeled mesoporous silica nanoparticles. ACS Nano 7, 9027–9039 (2013). [PubMed: 24083623]

181. Chen F et al. In vivo tumor vasculature targeted PET/NIRF imaging with TRC105(Fab)-conjugated, dual-labeled mesoporous silica nanoparticles. Mol. Pharm 11, 4007–4014 (2014). [PubMed: 24937108]

182. Guo J et al. Image-guided and tumor-targeted drug delivery with radiolabeled unimolecular micelles. Biomaterials 34, 8323–8332 (2013). [PubMed: 23932288]
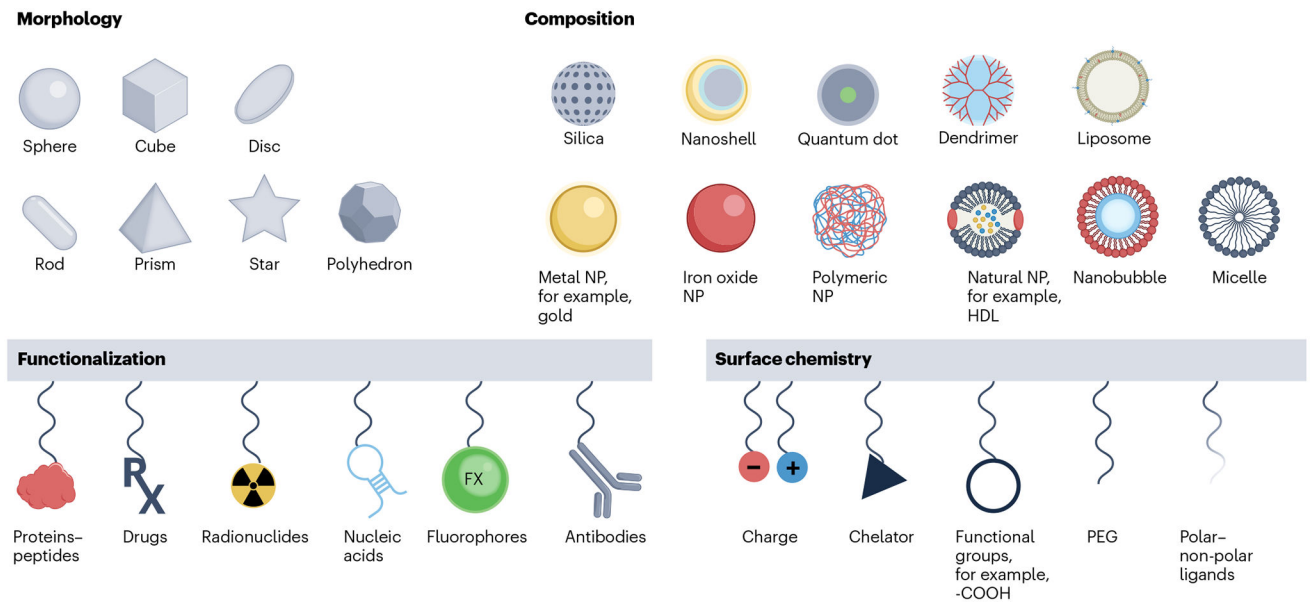
183. Goel S, Chen F, Ehlerding EB & Cai W Intrinsically radiolabeled nanoparticles: an emerging paradigm. Small 10, 3825–3830 (2014). [PubMed: 24978934]

184. Zhou M et al. A chelator-free multifunctional [64Cu]CuS nanoparticle platform for simultaneous micro-PET/CT imaging and photothermal ablation therapy. J. Am. Chem. Soc 132, 15351–15358 (2010). [PubMed: 20942456]

185. Zhao Y et al. Copper-64-alloyed gold nanoparticles for cancer imaging: improved radiolabel stability and diagnostic accuracy. Angew. Chem. Int. Ed 53, 156–159 (2014).

186. Zhan Y et al. Intrinsically zirconium-89 labeled Gd2O2S:Eu nanoprobes for in vivo positron emission tomography and gamma-ray-induced radioluminescence imaging. Small 12, 2872–2876 (2016). [PubMed: 27106630]

187. Zhan Y et al. Intrinsically zirconium-89-labeled manganese oxide nanoparticles for in vivo dual-modality positron emission tomography and magnetic resonance imaging. J. Biomed. Nanotechnol 14, 900–909 (2018). [PubMed: 29883560]

188. Chakravarty R et al. Intrinsically germanium-69-labeled iron oxide nanoparticles: synthesis and in-vivo dual-modality PET/MR imaging. Adv. Mater 26, 5119–5123 (2014). [PubMed: 24944166]

189. Liu T et al. Iron oxide decorated $MoS_2$ nanosheets with double PEGylation for chelator-free radiolabeling and multimodal imaging guided photothermal therapy. ACS Nano 9, 950–960 (2015). [PubMed: 25562533]

190. Campbell JL et al. Multimodal assessment of SERS nanoparticle biodistribution post ingestion reveals new potential for clinical translation of Raman imaging. Biomaterials 135, 42–52 (2017). [PubMed: 28486147]

191. Choi HS et al. Design considerations for tumour-targeted nanoparticles. Nat. Nanotechnol 5, 42–47 (2010). [PubMed: 19893516]

192. Hong G et al. In vivo fluorescence imaging with $Ag_2S$ quantum dots in the second near-infrared region. Angew. Chem. Int. Ed 51, 9818–9821 (2012).

193. Tang R et al. Tunable ultrasmall visible-to-extended near-infrared emitting silver sulfide quantum dots for integrin-targeted cancer imaging. ACS Nano 9, 220–230 (2015). [PubMed: 25560768]

194. Liu X, Braun GB, Qin M, Ruoslahti E & Sugahara KN In vivo cation exchange in quantum dots for tumor-specific imaging. Nat. Commun 8, 343 (2017). [PubMed: 28839238] This study describes the quenching of excess untargeted quantum dots through cation exchange with an etchant to facilitate renal clearance of metal ions and to further enhance tumour-specific detection.

195. Cao L et al. Competitive performance of carbon 'quantum' dots in optical bioimaging. Theranostics 2, 295–301 (2012). [PubMed: 22448196]

196. Hong G et al. Through-skull fluorescence imaging of the brain in a new near-infrared window. Nat. Photonics 8, 723–730 (2014). [PubMed: 27642366]

197. Wu TJ et al. Tracking the engraftment and regenerative capabilities of transplanted lung stem cells using fluorescent nanodiamonds. Nat. Nanotechnol 8, 682–689 (2013). [PubMed: 23912062]

198. Yoo JM, Kang JH & Hong BH Graphene-based nanomaterials for versatile imaging studies. Chem. Soc. Rev 44, 4835–4852 (2015). [PubMed: 25777530]

199. Zhong Y et al. Boosting the down-shifting luminescence of rare-earth nanocrystals for biological imaging beyond 1500 nm. Nat. Commun 8, 737 (2017). [PubMed: 28963467]

200. Hong G et al. Ultrafast fluorescence imaging in vivo with conjugated polymer fluorophores in the second near-infrared window. Nat. Commun 5, 4206 (2014). [PubMed: 24947309]

201. Li Z et al. Plant protein-directed synthesis of luminescent gold nanocluster hybrids for tumor imaging. ACS Appl. Mater. Interfaces 10, 83–90 (2018). [PubMed: 29220160]

202. Sun C et al. Fine-tuned H-ferritin nanocage with multiple gold clusters as near-infrared kidney specific targeting nanoprobe. Bioconjug. Chem 26, 193–196 (2015). [PubMed: 25594844]

203. Zhang Y, Hong H & Cai W Imaging with Raman spectroscopy. Curr. Pharm. Biotechnol 11, 654–661 (2010). [PubMed: 20497112]

204. Jokerst JV, Miao Z, Zavaleta C, Cheng Z & Gambhir SS Affibody-functionalized gold-silica nanoparticles for Raman molecular imaging of the epidermal growth factor receptor. Small 7, 625–633 (2011). [PubMed: 21302357]

205. Zavaleta CL et al. A Raman-based endoscopic strategy for multiplexed molecular imaging. Proc. Natl Acad. Sci. USA 110, E2288–E2297 (2013). [PubMed: 23703909]

206. Harmsen S et al. Surface-enhanced resonance Raman scattering nanostars for high-precision cancer imaging. Sci. Transl. Med 7, 271ra277 (2015).This work introduces a new generation of SERS imaging agents based on gold nanostars for accurate detection of macroscopic malignant lesions and microscopic foci.

207. Harmsen S et al. Rational design of a chalcogenopyrylium-based surface-enhanced resonance Raman scattering nanoprobe with attomolar sensitivity. Nat. Commun 6, 6570 (2015). [PubMed: 25800697]

208. Eremina OE et al. Expanding the multiplexing capabilities of Raman imaging to reveal highly specific molecular expression and enable spatial profiling. ACS Nano 10.1021/acsnano.2c00353 (2022).

209. Jiang X, Du B, Tang S, Hsieh JT & Zheng J Photoacoustic imaging of nanoparticle transport in the kidneys at high temporal resolution. Angew. Chem. Int. Ed 58, 5994–6000 (2019).

210. García-Álvarez R et al. Optimizing the geometry of photoacoustically active gold nanoparticles for biomedical imaging. ACS Photonics 7, 646–652 (2020).

211. Bouche M et al. Activatable hybrid polyphosphazene-AuNP nanoprobe for ROS detection by bimodal PA/CT imaging. ACS Appl. Mater. Interfaces 11, 28648–28656 (2019). [PubMed: 31321973]

212. Moore C & Jokerst JV Strategies for image-guided therapy, surgery, and drug delivery using photoacoustic imaging. Theranostics 9, 1550–1571 (2019). [PubMed: 31037123]

213. Dinish US et al. Single molecule with dual function on nanogold: biofunctionalized construct for in vivo photoacoustic imaging and SERS biosensing. Adv. Funct. Mater 25, 2316–2325 (2015).

214. Zhen X, Pu K & Jiang X Photoacoustic imaging and photothermal therapy of semiconducting polymer nanoparticles: signal amplification and second near-infrared construction. Small 17, e2004723 (2021). [PubMed: 33448155]

215. Cui D et al. Thermoresponsive semiconducting polymer nanoparticles for contrast-enhanced photoacoustic imaging. Adv. Funct. Mater 29, 1903461 (2019).

216. Yang K et al. Visualization of protease activity in vivo using an activatable photo-acoustic imaging probe based on CuS nanoparticles. Theranostics 4, 134–141 (2014). [PubMed: 24465271]

217. Chen YS, Zhao Y, Yoon SJ, Gambhir SS & Emelianov S Miniature gold nanorods for photoacoustic molecular imaging in the second near-infrared optical window. Nat. Nanotechnol 14, 465–472 (2019). [PubMed: 30833692]

218. Jokerst JV, Thangaraj M, Kempen PJ, Sinclair R & Gambhir SS Photoacoustic imaging of mesenchymal stem cells in living mice via silica-coated gold nanorods. ACS Nano 6, 5920–5930 (2012). [PubMed: 22681633]

219. Qian X, Shen S, Liu T, Cheng L & Liu Z Two-dimensional TiS(2) nanosheets for in vivo photoacoustic imaging and photothermal cancer therapy. Nanoscale 7, 6380–6387 (2015). [PubMed: 25786074]

220. Yang T et al. Size-dependent $Ag_2S$ nanodots for second near-infrared fluorescence/photoacoustics imaging and simultaneous photothermal therapy. ACS Nano 11, 1848–1857 (2017). [PubMed: 28117993]

221. Maji SK et al. Upconversion nanoparticles as a contrast agent for photoacoustic imaging in live mice. Adv. Mater 26, 5633–5638 (2014). [PubMed: 24913756]

222. Faria M et al. Minimum information reporting in bio–nano experimental literature. Nat. Nanotechnol 13, 777–785 (2018). [PubMed: 30190620] This perspective piece proposes a list of standards with respect to nanomaterial characterization and data reporting in an effort to improve reproducibility and to facilitate further discussion in the field of nano–bio science research.

223. Lammers T & Storm G Setting standards to promote progress in bio–nano science. Nat. Nanotechnol 14, 626 (2019). [PubMed: 31270443]

224. Florindo HF, Madi A & Satchi-Fainaro R Challenges in the implementation of MIRIBEL criteria on nanobiomed manuscripts. Nat. Nanotechnol 14, 627–628 (2019). [PubMed: 31270445]

225. Hühn J et al. Selected standard protocols for the synthesis, phase transfer, and characterization of inorganic colloidal nanoparticles. Chem. Mater 29, 399–461 (2017).

226. Leong HS et al. On the issue of transparency and reproducibility in nanomedicine. Nat. Nanotechnol 14, 629–635 (2019). [PubMed: 31270452]

227. Mendes BB et al. Nanodelivery of nucleic acids. Nat. Rev. Methods Primers 10.1038/s43586-022-00104-y (2022).

228. Li C A targeted approach to cancer imaging and therapy. Nat. Mater 13, 110–115 (2014). [PubMed: 24452345]

229. Kothapalli SR et al. Deep tissue photoacoustic imaging using a miniaturized 2-D capacitive micromachined ultrasonic transducer array. IEEE Trans. Biomed. Eng 59, 1199–1204 (2012). [PubMed: 22249594]

230. Ra H et al. Three-dimensional in vivo imaging by a handheld dual-axes confocal microscope. Opt. Express 16, 7224–7232 (2008). [PubMed: 18545427]

231. Park JH et al. Cooperative nanoparticles for tumor detection and photothermally triggered drug delivery. Adv. Mater 22, 880–885 (2010). [PubMed: 20217810]

232. Xie J et al. PET/NIRF/MRI triple functional iron oxide nanoparticles. Biomaterials 31, 3016–3022 (2010). [PubMed: 20092887]

233. Chien CY, Chuang HC, Huang SH, Lin WC & Huang HY A pilot study of segmental mandibulectomy with surgical navigation using fluorine-18 fluorodeoxyglucose positron-emission tomography/computed tomography. Laryngoscope 122, 2205–2209 (2012). [PubMed: 22674660]

234. Christensen A et al. Feasibility of real-time near-infrared fluorescence tracer imaging in sentinel node biopsy for oral cavity cancer patients. Ann. Surg. Oncol 23, 565–572 (2016). [PubMed: 26467454]

235. Higgins LM & Pierce MC Design and characterization of a handheld multimodal imaging device for the assessment of oral epithelial lesions. J. Biomed. Opt 19, 086004 (2014). [PubMed: 25104410]

236. Lee D et al. In vivo near infrared virtual intraoperative surgical photoacoustic optical coherence tomography. Sci. Rep 6, 35176 (2016). [PubMed: 27731390]

237. Lovell JF et al. Porphysome nanovesicles generated by porphyrin bilayers for use as multimodal biophotonic contrast agents. Nat. Mater 10, 324–332 (2011). [PubMed: 21423187]

238. Meershoek P et al. Three-dimensional tumor margin demarcation using the hybrid tracer indocyanine Green-(99m)Tc-nanocolloid: a proof-of-concept study in tongue cancer patients scheduled for sentinel node biopsy. J. Nucl. Med 60, 764–769 (2019). [PubMed: 30504140]

239. Sun IC et al. Heparin-coated gold nanoparticles for liver-specific CT imaging. Chemistry 15, 13341–13347 (2009). [PubMed: 19902441]

240. Nicolson F et al. Non-invasive in vivo imaging of cancer using surface-enhanced spatially offset Raman spectroscopy (SESORS). Theranostics 9, 5899–5913 (2019). [PubMed: 31534527]

241. Croissant JG & Brinker CJ Biodegradable silica-based nanoparticles: dissolution kinetics and selective bond cleavage. Enzymes 43, 181–214 (2018). [PubMed: 30244807]

242. Yang Y et al. Biodegradable nanostructures: degradation process and biocompatibility of iron oxide nanostructured arrays. Mater. Sci. Eng. C Mater Biol. Appl 85, 203–213 (2018). [PubMed: 29407149]

243. Tsoi KM, Dai Q, Alman BA & Chan WC Are quantum dots toxic? Exploring the discrepancy between cell culture and animal studies. Acc. Chem. Res 46, 662–671 (2013). [PubMed: 22853558]

244. Derfus AM, Chan WCW & Bhatia SN Probing the cytotoxicity of semiconductor quantum dots. Nano Lett 4, 11–18 (2004). [PubMed: 28890669]

245. Zhu S et al. A general route to make non-conjugated linear polymers luminescent. Chem. Commun 48, 10889–10891 (2012).

246. Zavaleta CL et al. Preclinical evaluation of Raman nanoparticle biodistribution for their potential use in clinical endoscopy imaging. Small 7, 2232–2240 (2011). [PubMed: 21608124]

247. van de Looij SM et al. Gold nanoclusters: imaging, therapy, and theranostic roles in biomedical applications. Bioconjug. Chem 33, 4–23 (2022). [PubMed: 34894666]

248. Wilhelm S et al. Analysis of nanoparticle delivery to tumours. Nat. Rev. Mater 1, 16014 (2016).

249. Li X, Anton N, Zuber G & Vandamme T Contrast agents for preclinical targeted X-ray imaging. Adv. Drug Deliv. Rev 76, 116–133 (2014). [PubMed: 25086373]

250. Hansen AE et al. Positron emission tomography based elucidation of the enhanced permeability and retention effect in dogs with cancer using copper-64 liposomes. ACS Nano 9, 6985–6995 (2015). [PubMed: 26022907] This report investigates the EPR effect-induced accumulation of NPs in solid tumours of large animals using nanocarrier-radiotracers via PET/CT imaging.

251. Miller MA et al. Tumour-associated macrophages act as a slow-release reservoir of nano-therapeutic Pt(IV) pro-drug. Nat. Commun 6, 8692 (2015). [PubMed: 26503691]

252. Hui JZ & Tsourkas A Optimization of photoactive protein Z for fast and efficient site-specific conjugation of native IgG. Bioconjug. Chem 25, 1709–1719 (2014). [PubMed: 25121619]

253. Anselmo AC & Mitragotri S Nanoparticles in the clinic: an update post COVID-19 vaccines. Bioeng. Transl. Med 6, e10246 (2021). [PubMed: 34514159]

254. Miyasato DL, Mohamed AW & Zavaleta C A path toward the clinical translation of nano-based imaging contrast agents. Wiley Interdiscip. Rev. Nanomed. Nanobiotechnol 13, e1721 (2021). [PubMed: 33938151]

255. Shen Z, Wu A & Chen X Iron oxide nanoparticle based contrast agents for magnetic resonance imaging. Mol. Pharm 14, 1352–1364 (2017). [PubMed: 27776215]

256. Jain S, Hirst DG & O'Sullivan JM Gold nanoparticles as novel agents for cancer therapy. Br. J. Radiol 85, 101–113 (2012). [PubMed: 22010024]

257. Llop J & Lammers T Nanoparticles for cancer diagnosis, radionuclide therapy and theranostics. ACS Nano 10.1021/acsnano.1c09139 (2021).

**Morphology**

Sphere Cube Disc

Rod Prism Star Polyhedron

**Composition**

Silica Nanoshell Quantum dot Dendrimer Liposome

Metal NP, for example, gold | Iron oxide NP | Polymeric NP | Natural NP, for example, HDL | Nanobubble | Micelle

**Functionalization**

Proteins–peptides | Drugs | Radionuclides | Nucleic acids | Fluorophores | Antibodies

**Surface chemistry**

Charge | Chelator | Functional groups, for example, -COOH | PEG | Polar–non-polar ligands

**Fig. 1 |. Design principles of nanomaterial-based contrast agents for various imaging modalities and biomedical applications.**
The physicochemical properties of nano-based contrast agents are generally described by their core and hydrodynamic diameter, chemical composition, shape, surface chemistry and functionalization. These agents are designed and optimized for major bioimaging modalities that produce contrast based on X-rays, radioactive decay, magnetism, optical photons and acoustics. These agents, in conjunction with the appropriate imaging techniques, are applied to provide structural and functional information of the disease in question. HDL, high-density lipoprotein; NP, nanoparticle; PEG, polyethylene glycol.
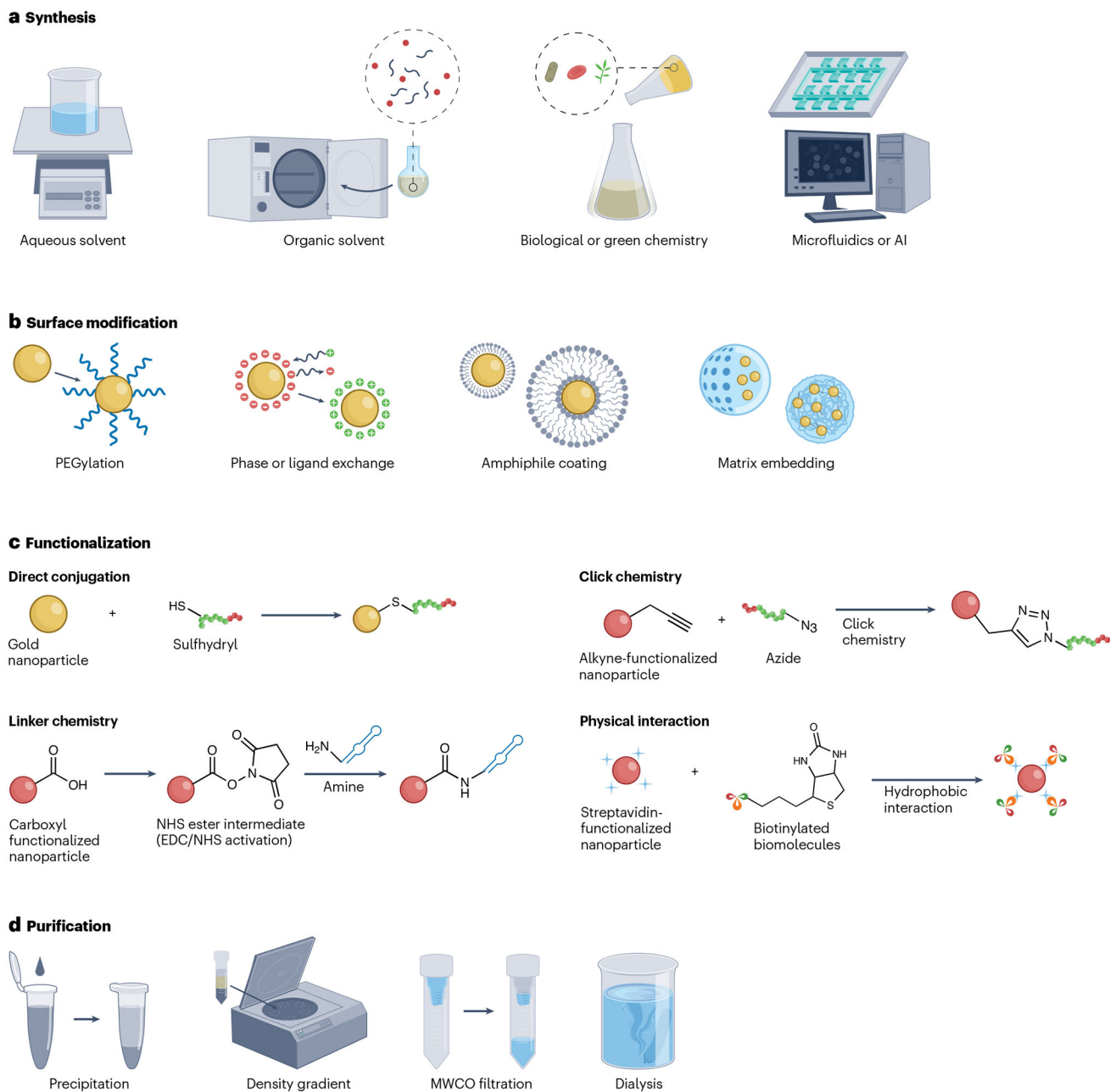
**Fig. 2 |. Overview of the approaches used for synthesizing, conjugating and purifying nanomaterial-based contrast agents.**

**a**, Nano-based contrast agents have traditionally been synthesized using aqueous and organic solvents. Recent syntheses based on green chemistry, biological precursors, microfluidics and artificial intelligence (AI) have become increasingly utilized for nanomaterial fabrication. **b,c**, Surface modification (part **b**) and/or functionalization (part **c**) is performed to render the agents viable for bioimaging applications. **d**, The agents are further purified to remove impurities before in vitro and in vivo evaluation. EDC, *N*-ethyl-*N*'-(3-dimethylaminopropyl) carbodiimide; MWCO, molecular weight cut-off; NHS, *N*-hydroxysuccinimide; PEG, polyethylene glycol. Part **c** reprinted from ref. 86, CC BY 4.0.
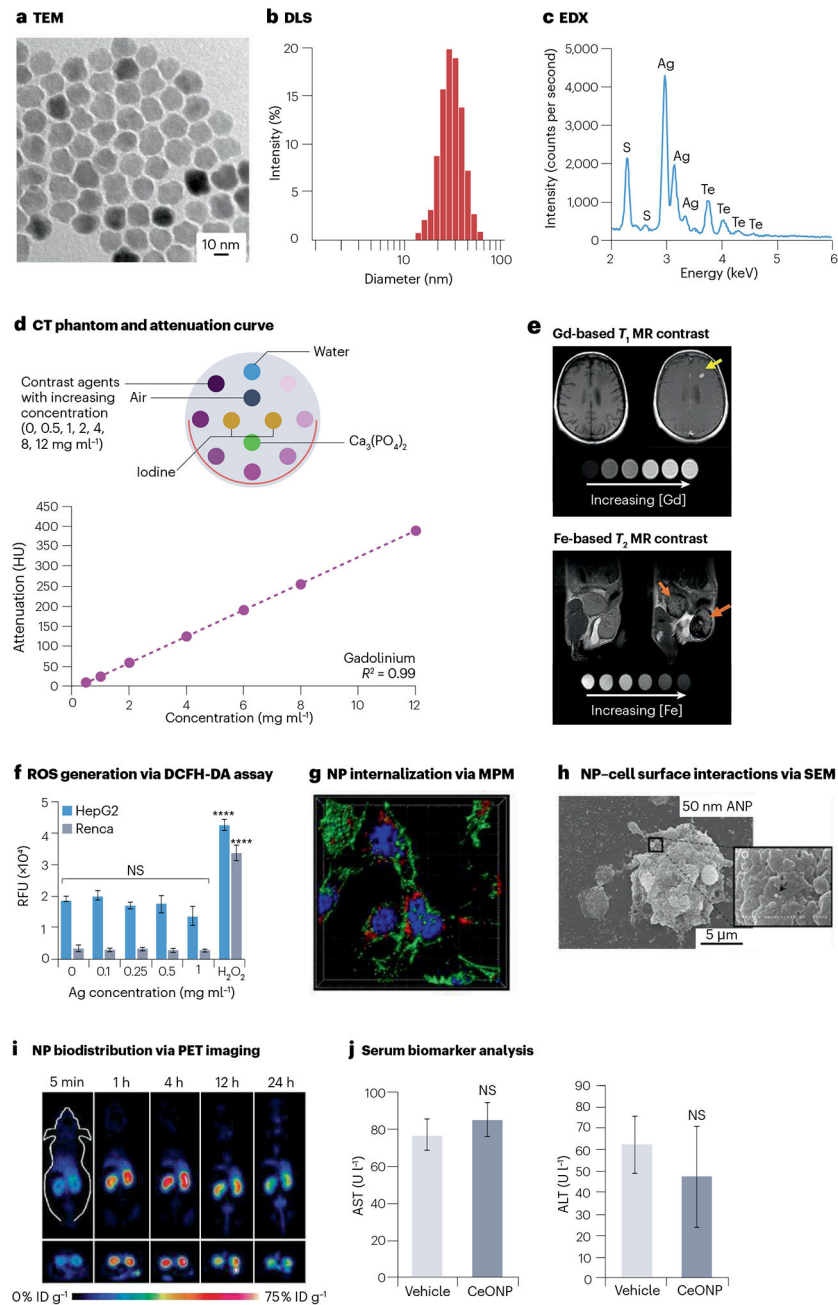
**Fig. 3 |. Examples of physical characterization, imaging assessments and biological interactions of nanomaterial-based contrast agents.**

**a**, Transmission electron microscopy (TEM) assesses the nanoparticle (NP) core diameter. **b**, Dynamic light scattering (DLS) measures the NP hydrodynamic diameter. **c**, Energy-dispersive X-ray spectroscopy (EDX) identifies the elemental composition of NP. **d**, Example of a computed tomography (CT) phantom (inset) and attenuation curve derived from the corresponding CT phantom images. **e**, NPs based on gadolinium (Gd) and iron (Fe) are commonly used as $T_1$-weighted and $T_2$-weighted contrast agents for magnetic resonance imaging (MRI), respectively. Yellow arrow indicates brightening of a brain metastasis due

to Gd via $T_1$-weighted MRI. Orange arrows indicate darkening of mammary gland tumours due to Fe via $T_2$-weighted MRI. **f**, In vitro intracellular reactive oxygen species (ROS) generation is commonly investigated by the $2',7'$-dichlorofluorescein diacetate (DCFH-DA) assay. Data are presented as mean ± s.d. \*\*\*\*$P < 0.0001$. **g**, Subcellular resolution multiphoton microscopy (MPM) evaluates cellular internalization of the NP. **h**, Scanning electron microscopy (SEM) visualizes the interactions between the NP and cell surface. **i**, In vivo biodistribution (percentage of injected dose per gram of tissue, %ID $g^{-1}$) is easily determined using positron emission tomography (PET) imaging with radiolabelled NPs. **j**, Serum biomarkers from blood samples indicate potential NP toxicity and organ damages, such as alanine transaminase (ALT) and blood urea nitrogen (BUN) for liver and kidney functions, respectively. AST, aspartate transferase; CeONP, ceriumoxide nanoparticles; HepG2, hepatocellular carcinoma; NS, not significant; Renca, renal cell carcinoma; RFU, relative fluorescence units. Parts **a** and **b** reprinted from ref. 91, Springer Nature Limited. Parts **c** and **f** reprinted with permission from ref. 5. Copyright 2022 American Chemical Society. Part **d** reprinted from ref. 110, Springer Nature Limited. Part **e** reprinted with permission from ref. 112, Wiley. Part **g** reprinted from ref. 123, Springer Nature Limited. Part **h** reprinted from ref. 124, Springer Nature Limited. Part **i** reprinted from ref. 125, CC BY 4.0. Part **j** reprinted with permission from ref. 64. Copyright 2021 American Chemical Society.
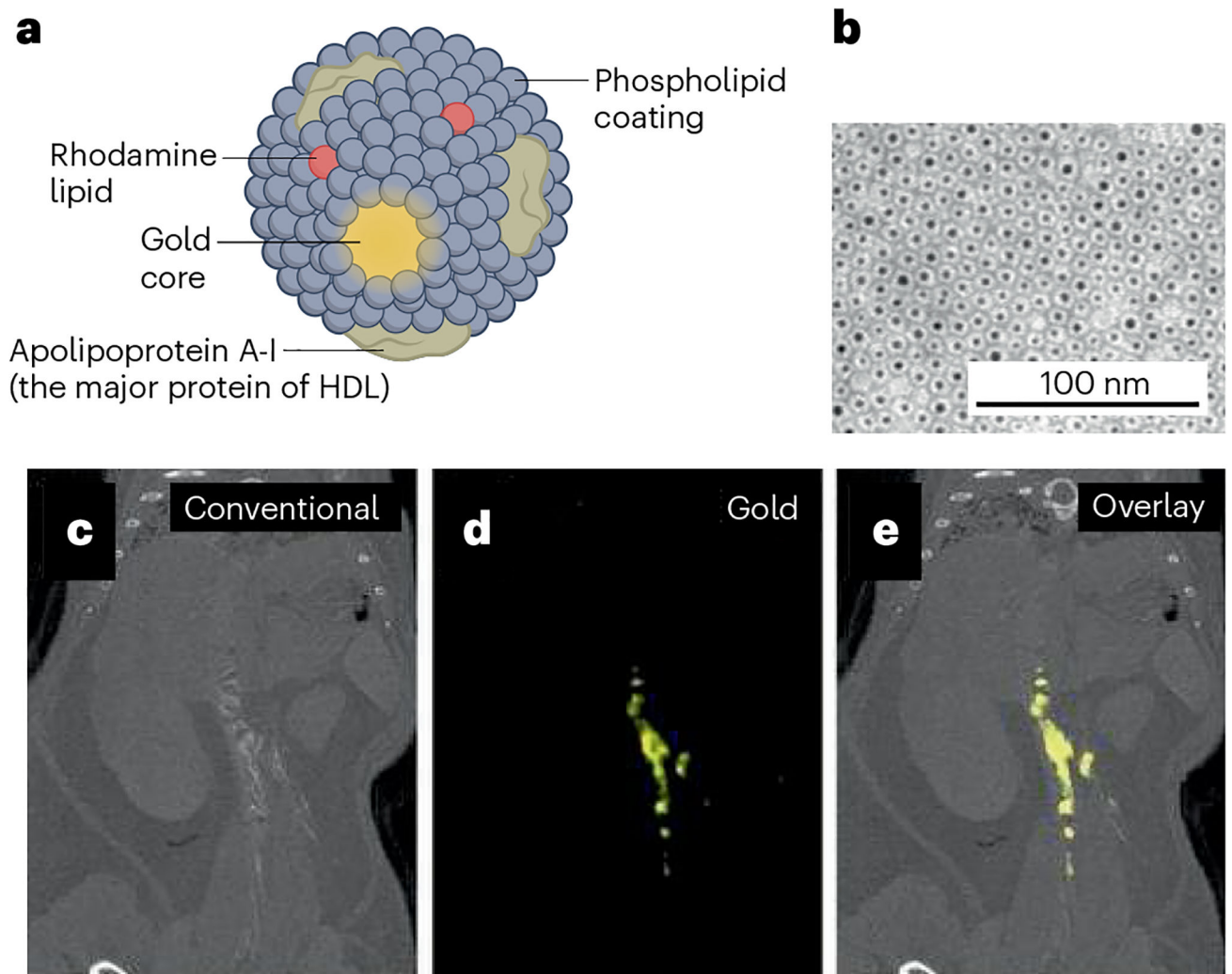
**Fig. 4 |. Spectral computed tomographic imaging of atherosclerotic plaque composition with gold-loaded high-density lipoprotein.**

**a**, Schematic illustration of macrophage-targeted nanoparticle computed tomographic (CT) contrast agent based on Au-high-density lipoprotein (Au-HDL). **b**, Au-HDL on a negative-stain micrograph from transmission electron microscopy. **c**, Conventional CT image of thorax and abdomen in a mouse with atherosclerosis after injection of Au-HDL. **d**, Spectral CT image showing signal from gold and accumulation of Au-HDL in the arteries of the mouse. **e**, Overlay of conventional and gold images. Reprinted with permission from ref. 136, Radiological Society of North America.
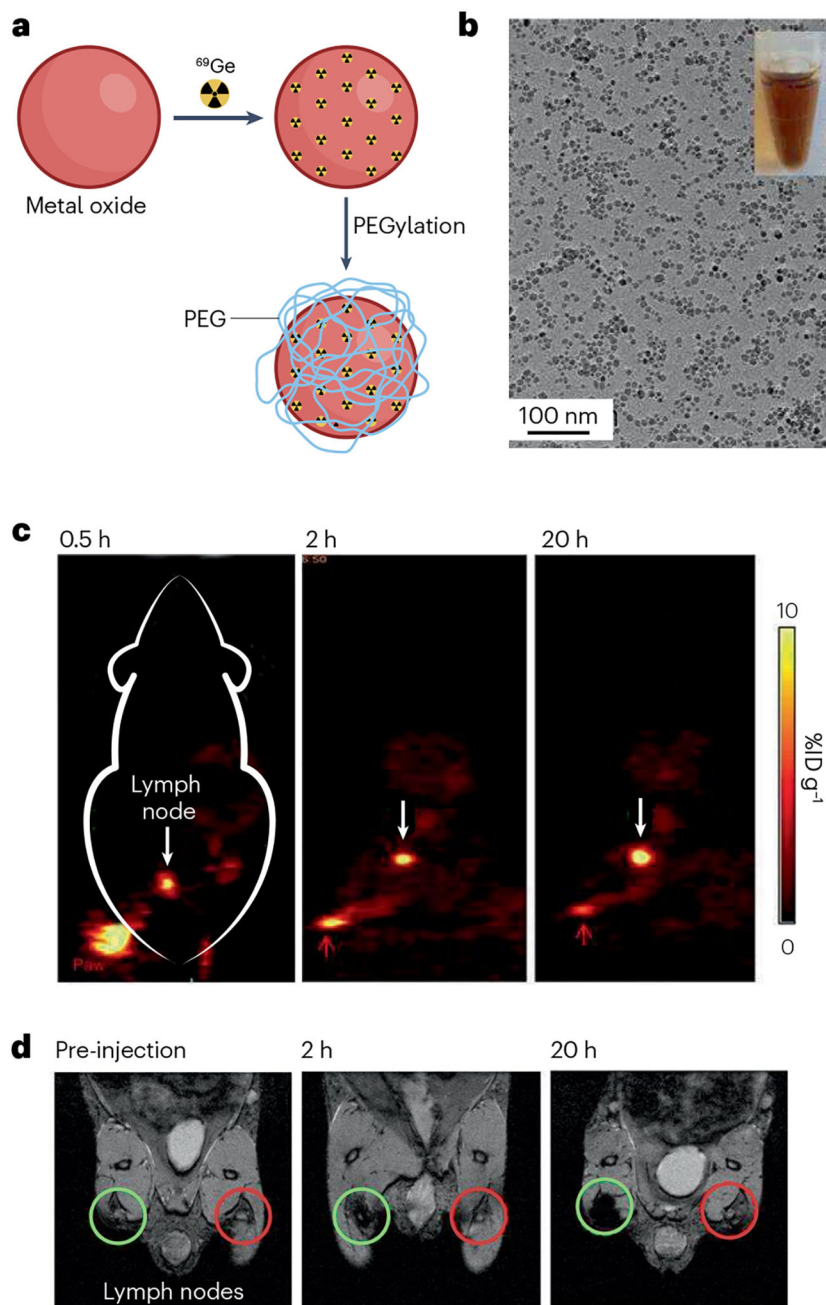
**Fig. 5 |. Superparamagnetic iron oxide nanoparticles labelled with $^{69}$Ge for lymph node mapping via positron emission tomography and MRI.**

**a**, Schematic illustration of chelator-free synthesis of $^{69}$Ge-iron oxide nanoparticles (IONPs). **b**, Micrograph of IONPs from transmission electron microscopy. **c**, Lymph node (white arrow) imaging with positron emission tomography after injection of $^{69}$Ge-IONPs into left paw (red arrow) of a mouse. **d**, Lymph node (green circle) mapping with MRI before and after injection of $^{69}$Ge-IONPs into left paw of a mouse. Contralateral lymph node is indicated by red circle. %ID g$^{-1}$, percentage of injected dose per gram of tissue; PEG, polyethylene glycol. Reprinted with permission from ref. 188, Wiley.
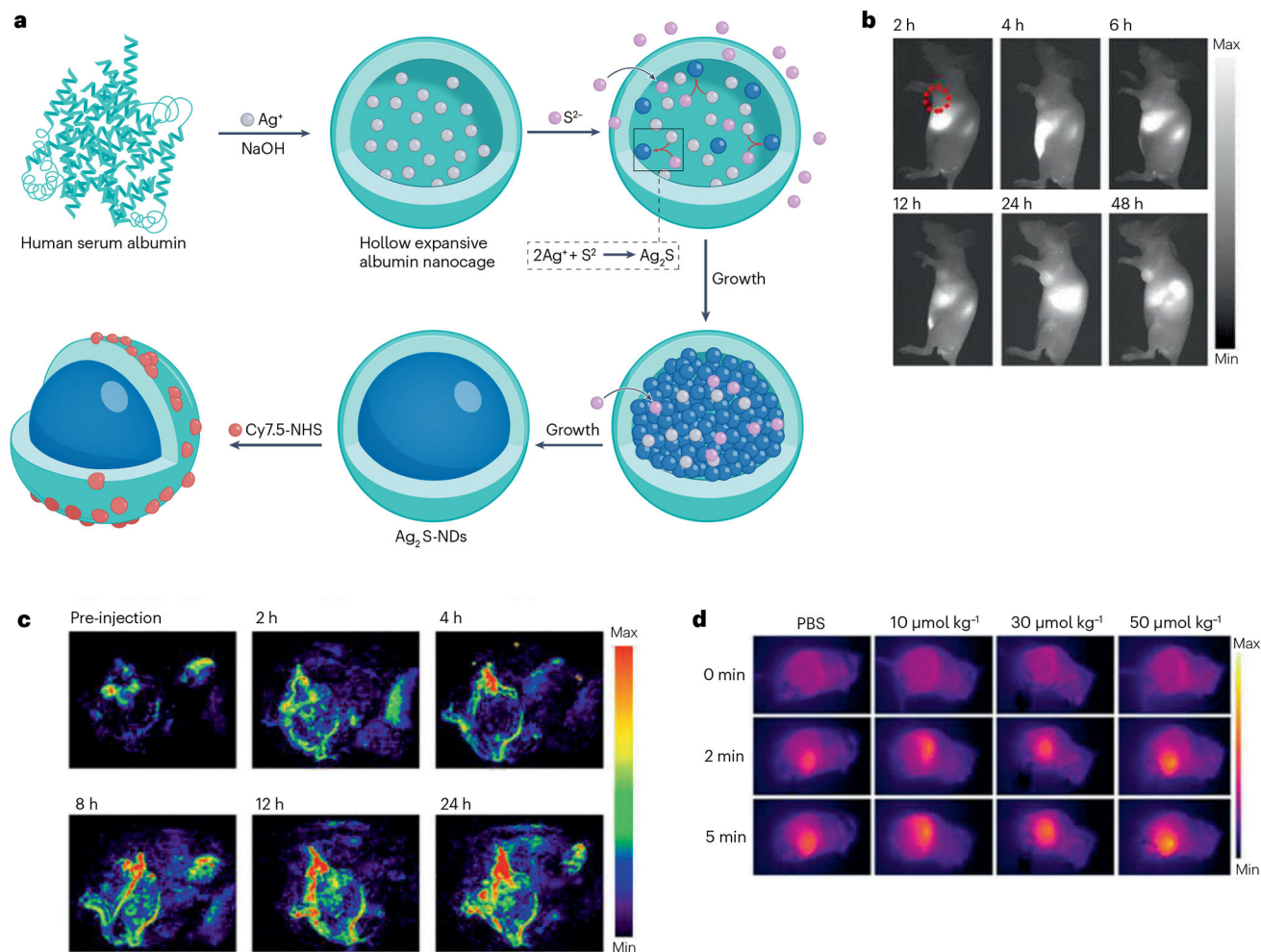
**Fig. 6 |. Ag₂S nanoparticles with theranostic functionality for tumour imaging and treatment.**
**a**, Schematic illustration of synthesis of serum albumin-coated Ag₂S nanoparticles. **b,c**, In vivo tumour detection via near-infrared-II fluorescence imaging (part **b**) and photoacoustic imaging (part **c**). **d**, Infrared thermography of tumours showing elevated temperature when irradiated with a near-infrared laser. NDs, nanodots; NHS, *N*-hydroxysuccinimide; PBS, phosphate-buffered saline. Adapted with permission from ref. 220. Copyright 2017 American Chemical Society.

**Table 1 |**

Features of commonly used medical imaging modalities and relevant nano-based contrast agents

| Imaging modality | Spatial resolution | Temporal resolution | Sensitivity | Penetration depth | Example nanomaterials |
|---|---|---|---|---|---|
| **X-ray contrast agents** | | | | | |
| Computed tomography | 25 μm–5 mm | Seconds to minutes | $10^{-3}$ M | No limit | Metal NPs (iodine, gold, tantalum, bismuth, lanthanides) |
| Mammography | 50 μm–1 mm | Seconds | $10^{-3}$ M | No limit | Metal NPs (iodine, silver, molybdenum, gold) |
| **Nuclear contrast agents** | | | | | |
| Positron emission tomography | 1–5 mm | Seconds to minutes | $10^{-10}$ M | No limit | $^{89}$Zr-labelled HDL, $^{64}$Cu-labelled CuS NPs |
| Single photon emission computed tomography | 1–10 mm | minutes | $10^{-10}$ M | No limit | $^{99m}$Tc-labelled IONPs/liposomes |
| **Magnetic contrast agents** | | | | | |
| Magnetic resonance imaging | 25 μm–5 mm | Minutes to hours | $10^{-5}$ M | No limit | IONPs, Gd-dendrimers, MnO NPs |
| Magnetic particle imaging | 500 μm | Milliseconds | $10^{-6}$ M | No limit | IONPs, FeCo NPs |
| **Optical contrast agents** | | | | | |
| Fluorescence imaging | 1–3 mm | Seconds to minutes | $10^{-12}$ M | <1–5 cm | QDs, AuNPs, carbon nanotubes, dye-loaded micelle |
| Photoacoustic imaging | 50 μm–1 mm | Seconds to minutes | $10^{-11}$ M | <5 cm | AuNPs, semiconducting polymer |
| SERS | 1 μm–1 mm | Seconds to hours | $10^{-15}$ M | <0 mm | Gold and SERS NPs |
| Ultrasound | 0.1–1 mm | Seconds | $10^{-4}$ M | 5–30 cm | Lipid, polymer or protein-coated nanobubbles |

Values listed span clinical and preclinical systems. Sensitivities are on a per element basis. HDL, high-density lipoprotein; IONPs, iron oxide nanoparticles; NP, nanoparticle; QD, quantum dot; SERS, surface-enhanced Raman spectroscopy.

**Table 2 |**

Summary of several nanomaterial-based contrast agents that are approved or trialled in the clinic

| Imaging mode | Candidate | Approved trade name or ClinicalTrials.gov identifier | Phase |
|---|---|---|---|
| PET/SPECT | $^{99m}$Tc sulfur colloids | Technecoll (USA) | Approved |
| PET/SPECT | $^{125}$I albumin colloids | Jeanatope (USA) | Approved |
| PET/SPECT | $^{99m}$Tc SnF$_2$ colloids | Hepatate (France) | Approved |
| PET/SPECT | $^{99m}$Tc Re$_2$O$_7$ colloids | Nanocis (EU) | Approved |
| PET/SPECT | $^{89}$Zr cRGDY silica | NCT03465618 | 1 |
| PET/SPECT | Gd liposome | NCT05453539 | 1 |
| MRI | Iron oxides | Feridex (USA) | Approved |
| MRI | Polysiloxane (AGuIX) | NCT04789486 | 1 |
| Fluorescence | cRGDY silica (C dots) | NCT02106598 | 2 |
| Fluorescence | pH-sensitive micelle (ONM-100) | NCT05048082 | 2 |
| X-ray CT | Hafnium oxide (NBTXR3) | NCT04892173 | 3 |
| X-ray CT | Ethiodized oil | Lipiodol (USA) | Approved |

CT, computed tomography; MRI, magnetic resonance imaging; PET, positron emission tomography; SPECT, single photon emission computed tomography.